Smooth muscle enriched long non-coding RNA (SMILR) regulates cell proliferation

Citation for published version:
Ballantyne, MD, Pinel, K, Dakin, R, Vesey, AT, Diver, L, Mackenzie, R, Garcia, R, Welsh, P, Sattar, N, Hamilton, G, Joshi, N, Dweck, MR, Miano , JM, McBride, MW, Newby, DE, McDonald, RA & Baker, AH 2016, 'Smooth muscle enriched long non-coding RNA (SMILR) regulates cell proliferation', *Circulation*, vol. 133, no. 21, pp. 2050-2065. https://doi.org/10.1161/CIRCULATIONAHA.115.021019

Digital Object Identifier (DOI):
10.1161/CIRCULATIONAHA.115.021019

Link:
Link to publication record in Edinburgh Research Explorer

Document Version:
Peer reviewed version

Published In:
Circulation

DOI: 10.1161/CIRCULATIONAHA.115.021019

Smooth Muscle Enriched Long Non-Coding RNA (*SMILR*) Regulates Cell Proliferation

Running title: *Ballantyne et al.; SMILR lncRNA regulates cell proliferation*

Margaret D. Ballantyne, MRes[1,2]; Karine Pinel, PhD[2]; Rachel Dakin, PhD[1]; Alex. T. Vesey, MD[2]; Louise Diver, PhD[1]; Ruth Mackenzie, PhD[1]; Raquel Garcia, PhD[1]; Paul Welsh, PhD[1]; Naveed Sattar, MD, PhD[1]; Graham Hamilton, PhD[3]; Nikhil Joshi, MD, PhD[2]; Marc R. Dweck, MD, PhD[2]; Joseph M. Miano, PhD[4]; Martin W. McBride, PhD[1]; David E. Newby, MD, PhD[2]; Robert. A. McDonald, PhD[1,2]; Andrew H. Baker, PhD[1,2]

[1]BHF Glasgow Cardiovasc Res Centre, University of Glasgow, Glasgow, United Kingdom; [2]British Heart Foundation/University of Edinburgh Centre for Cardiovascular Science, Edinburgh, United Kingdom; [3]Glasgow Polyomics, College of Medical, Veterinary and Life Sciences, The University of Glasgow, Glasgow, United Kingdom; [4]Aab Cardiovasc Res Institute, University of Rochester School of Medicine and Dentistry, Rochester, NY

Address for Correspondence:

Andrew H. Baker, PhD
BHF Glasgow Cardiovasc Res Centre
126 University Place
University of Glasgow
Glasgow, United Kingdom
Tel: +44 0141 330 1977
Fax: +44 0141 330 3360
Email: andrew.h.baker@glasgow.ac.uk

Journal Subject Terms: Atherosclerosis; Vascular Disease; Restenosis

Abstract

***Background*—**Phenotypic switching of vascular smooth muscle cells (VSMCs) from a contractile to a synthetic state is implicated in diverse vascular pathologies including atherogenesis, plaque stabilisation, and neointimal hyperplasia. However, very little is known as to the role of long non coding RNA (lncRNA) during this process. Here we investigated a role for long non-coding (lnc)RNAs in VSMC biology and pathology.

***Methods and Results*—**Using RNA-sequencing, we identified >300 lncRNAs whose expression was altered in human saphenous vein (HSV) VSMCs following stimulation with IL1α and PDGF. We focused on a novel lncRNA (Ensembl: RP11-94A24.1) which we termed smooth muscle induced lncRNA enhances replication (*SMILR*). Following stimulation, *SMILR* expression was increased in both the nucleus and cytoplasm, and was detected in conditioned media. Furthermore, knockdown of *SMILR* markedly reduced cell proliferation. Mechanistically, we noted that expression of genes proximal to *SMILR* were also altered by IL1α/PDGF treatment, and HAS2 expression was reduced by *SMILR* knockdown. In human samples, we observed increased expression of *SMILR* in unstable atherosclerotic plaques and detected increased levels in plasma from patients with high plasma C-reactive protein.

***Conclusions*—**These results identify *SMILR* as a driver of VSMC proliferation and suggest that modulation of *SMILR* may be a novel therapeutic strategy to reduce vascular pathologies.

Key words: microRNA; atherosclerosis; non-coding RNA; vascular smooth muscle; proliferation; long non-coding RNA

Introduction

Vessel wall remodelling is an integral pathological process central to cardiovascular diseases including atherogenesis, plaque rupture and neointimal hyperplasia associated vein graft failure and in-stent restenosis [1, 2]. Resident vascular smooth muscle cells (VSMC) are typically quiescent and contractile in the normal physiological state. However, following pathological or iatrogenic vascular injury, the release of cytokines and growth factors from VSMC, aggregated platelets and inflammatory cells on the damaged intimal surface, leads to “phenotypic switching" of VSMC and the adoption of a more synthetic, pro-proliferative and pro-migratory state [3]. In the setting of the pathological injury of atherosclerosis, VSMCs not only contribute to the atherogenic process itself but can also engender plaque stabilisation through the generation of a thick-capped fibroatheroma. For acute iatrogenic vascular injury, over exuberant proliferation of VSMC subpopulations promotes neointimal hyperplasia leading to luminal narrowing such as seen in vein graft failure or in-stent restenosis [4]. Phenotypic switching of VSMCs and release of cytokines and growth factors are therefore critical in vascular disease and understanding the mechanisms involved is critical to gain insights into pathology and identify new opportunities for therapies.

The highly conserved IL1α and PDGF pathways play prominent roles in VSMC-associated pathologies [1, 5]. IL1α is a central mediator in the cytokine cascade and a potent activator of vascular cytokine production. Furthermore, previous studies have demonstrated that ligation injury result in reduced neointimal formation in IL-1 receptor knockout mice [6]. Downstream mediators include the signalling molecules MEKK1, p38 and the transcription factor NF-κB that activate mediators of inflammation and cellular migration [7]. PDGF is a potent mitogen and chemoattractant and expression is increased following vascular injury [8]. Conversely a reduction in PDGF expression reduces intimal thickening and cellular content of the neointima [9]. Activation of both IL1α and PDGF signalling pathways simultaneously can activate common downstream targets leading to additive or synergistic effects. This includes activation of NFκB leading to the up-regulation of MMP 3 and 9 [10]: genes critical in the development of vasculoproliferative pathologies.

Over the past decade, there has been substantial interest in determining the complex interactions between hierarchical levels of gene regulation. Up to 90% of the human genome is transcribed at different developmental stages and only approximately 2% of RNA molecules are translated into protein [11]. The functional complexity of organisms therefore appears to be reliant upon non-coding RNA molecules. Non-coding RNAs are subdivided into several classes, including microRNA (miRNA) and long non-coding RNA (lncRNA). MiRNAs are abundantly expressed in vascular tissues and play an important role in vascular pathology. Interestingly, recent studies have demonstrated that miRNAs are capable of being released into the blood from injured cells. These miRNAs are relatively stable and have been reported as biomarkers for several disease states including myocardial infarction [12] and heart failure[13, 14]. While the role of miRNAs is reasonably established in the setting of cardiovascular pathology, relatively little is known about the role of lncRNAs. LncRNAs are capable of regulating target DNA, RNA and protein at the pre and post-transcriptional level. It is becoming clear that lncRNAs play a pivotal role in cellular physiology and pathology via localisation in sub populations of cells and through highly controlled temporal expression [15]. However, detailed insights into their regulation and biological roles are only beginning to emerge. In the vascular setting, *SENCR* and *MALAT1* have been implicated in the control of vascular cell migration and endothelial cell sprouting, respectively [16], [17]. Interestingly, *SENCR* is implicated in phenotypic switching of VSMCs to a more pro-migratory phenotype as knockdown of this lncRNA downregulates contractile genes [17]. A greater understanding of lncRNAs in quiescent and proliferative VSMCs may provide valuable insight into the specific roles of lncRNAs in response to pathological processes.

Methods

Human tissue samples

Surplus human saphenous vein tissue was obtained from patients undergoing CABG. Carotid plaques were obtained from patients undergoing endarterectomy following an acute and symptomatic neurovascular event. Human plasma samples were utilised from a previously published study: Carotid Ultrasound and Risk of Vascular disease in Europeans and South Asians (CURVES) [2]. All patients gave their written, informed consent. All procedures had local ethical approval (06/S0703/110, 12/WS/0227, 09/S0703/118 and 12/NW/0036). All studies were approved by East and West Scotland Research Ethics Committees and all experiments were conducted according to the principles expressed in the Declaration of Helsinki.

Tissue and Cell culture

All cells were maintained at 37°C in a humidified atmosphere containing 5% CO_2. Primary human saphenous vein derived endothelial cells (HSVECs) were isolated by a modified version of the protocol described by Jaffe and colleagues [18] and maintained in large vessel endothelial cell culture medium. supplemented with 20% FCS (Life Technologies, Paisley, UK). Primary human saphenous vein derived smooth muscle cells (HSVSMC) were isolated from medial explants [19] and maintained in Smooth Muscle Cell Growth Medium 2 (PromoCell, Heidelberg, Germany) with supplements. Human coronary artery VSMC were purchased from Lonza (Basel, Switzerland) and maintained in VSMC media as above.

Sample preparation for RNA-seq library construction and analysis

HSVSMC were plated, quiesced in medium containing 0.2% fetal calf serum for 48 hour before the stimulation with 10 ng/ml IL1α, 20 ng/ml PDGF (R&D Systems) or a combination of both for 72 hours. Total RNA was processed through miRNeasy kit (Qiagen, Hilden, Germany) following the manufacturer's instructions, treated with DNAse 1 (amplification grade; Sigma, St. Louis, USA) in order to eliminate genomic DNA contamination and quantified using a NanoDrop ND-1000 Spectrophotometer (Nano-Drop Technologies, Wilmington, DE, USA). Following bioanalyzer quality control for RNA integrity number (RIN) values >8, RNA-seq was performed on ribosomal-depleted RNA using an Illumina Hiseq platform by Beckman Coulter Genomics. Paired-end sequencing was carried out with a read depth of 70 million (n=4/group). RNA-seq reads were processed and trimmed to ensure quality and remove adapter sequences using Flexbar [20] and mapped to the Ensembl annotation of GRCh37.75 using the TopHat2 version 2.0.9 [21]. The transcriptome was assembled from the aligned reads and quantified using Cufflinks version 2.2.1 [22]. The differential expression levels between the groups was assessed using Cuffdiff version 2.2.1 [23]. The data set are deposited in the GEO repository, study number GSE69637. The biotype of each transcript was annotated according to the Ensembl database. Normalisation and statistical analysis of differentially expressed transcripts were carried out using edgeR and data filtered to find transcripts that were differentially expressed ($p<0.01$) between 0.2% media and each treatment group. Differentially expressed lncRNAs, between control and both IL1α/PDGF treatment, were explored using more stringent criteria ($p<0.01$, $FDR<0.01$, $LogFC>2$) and filtered according to transcript abundance ($FPKM>1$ in at least one group). Data outputs such as pie charts and heatmaps were generated using R. IPA analysis was carried out using protein coding genes differentially expressed ($FDR<0.01$) from Edge R analysis.

Assessment of RNA secretion from HSVSMC

RNA extraction on conditioned HSVSMC media was performed using a standard volume (2 mL). The conditioned media was first centrifuged (10 min; 2000 g; 4°C) to remove all cells and debris. After addition of 1.4 mL of QIAzol (Qiagen), 3 µL of c.elegans total RNA at 25 ng/µL was added to each sample. Following 5-min incubation at RT, 140 µL of chloroform was added and samples centrifuged (15 min; 15000 g; 4°C). The clear upper aqueous phase was used to isolate RNA using miRNEasy mini kit (Qiagen) as previously described with alteration of the final wash step (75 % ethanol in DEPC water). Different quantities of total RNA were spiked and a dose response effect was observed (**Suppl. Figure 1A**). The quality of the amplicon was assessed via analysis of melting curves (**Suppl. Figure 1B**) and subsequent visualisation on agarose gel (**Suppl. Figure 1C**). This showed a unique amplification product corresponding to the cDNA fragment of *ama-1*. Due to the correlation observed between quantity of spike-in and *ama-1* expression (**Suppl. Figure 1D**), we utilised 75 ng in all subsequent extractions. This amount allowed reproducibility of our method, with the Ct values of *ama-1* being 29.4±0.3 across 5 separate extractions in non-conditioned media (**Suppl. Figure 1E**).

Gene expression quantitative RealTime-PCR (qRT-PCR)

For gene expression analysis, cDNA for mRNA analysis was obtained from total RNA using the Multiscribe Reverse Transcriptase (Life technologies, Paisley, UK). qRT-PCR was performed using Power SYBR green (Life Technologies) with custom PCR primers (Eurofins MWG, Ebersberg, Germany), the specificity of these primers was confirmed by performing a melting curve and running their PCR produce on a gel (**Suppl. Table 1** – primer sequences). Ubiquitin C (UBC) was selected as housekeeping gene due to its stability across all groups studied. Fold-changes were calculated using the 2-ΔΔCt method 23.

Statistical Analysis

Statistical analysis was performed according to figure legends. Data in graphs are shown on relative expression scales as referenced by [24]. Data are given as both mean ± standard deviation (StDev) (shown as bars and whiskers) and also as the individual points in order to clearly represent the data. Note that as the relative expression scale is inherently skewed, the bar indicate the geometric mean of the relative expression fold change with the StDev whiskers denoting the relative expression fold change equivalent to an increase of one StDev above the mean on the log transformed scale. All statistical analysis is performed on the dCt scale (a logarthmic transformation of the data shown on the RQ in the plots)[24]. No evidence of unequal variances across groups was found for any of analyses of the dCt scale data using Levene's test on minitab version 17 prior to statistical analysis. Comparisons between 2 groups were analysed using 2-tailed unpaired or paired Student's t test. One-way ANOVA with Tukey's post hoc or one way ANOVA multiple comparison test for pooled samples, via Graph Pad Prism version 5.0, was used for comparisons among 3 or more groups. Statistical significance is denoted by a P value of less than 0.05.

Results

Induction of inflammatory and cell cycle pathways by IL1α and PDGF

We sought to identify lncRNAs that are regulated during the induction of proliferative and inflammatory pathways in HSVSMC. RNAs were identified using RNA-seq of HSVSMC treated for 72 h (**Figure 1A**). Activation of the IL1α and PDGF signalling pathways was confirmed by presence of the inflammatory microRNA miR-146a (**Figure 1B**) and induction of VSMC proliferation (**Figure 1C**). The RNA-sequencing obtained an average of 70 million reads per sample; with 93.5% aligning to the GRCh37 genome reference files. The majority of reads, under all conditions, corresponded to mRNA (49.6±0.48 %; **Figure 1D** and **Suppl. Figure 2A**). To identify the biological function, networks, and canonical pathways that were affected by VSMC stimulation, we performed Ingenuity Pathway Analysis (IPA) after RNA-seq analysis. IPA confirmed the mRNAs with altered expression following IL1α treatment were significantly enriched in pathways related to cellular movement and inflammatory disease (**Suppl. Table 2**), while PDGF stimulation led to the marked enrichment in cell cycle pathways (**Suppl. Table 3**). Interestingly, co-stimulation led to enrichment in cell cycle and cardiovascular development pathways (**Suppl. Table 4**). Further analysis of differentially expressed mRNAs with a stringent cut off of FDR<0.01 identified 518 protein coding genes altered following IL1α treatment and 540 following PDGF treatment. Notably, dual stimulation altered 1133 known protein-coding genes with 480 uniquely associated with dual stimulation and not affected by IL1α or PDGF treatment alone (**Figure 1E** and **Suppl. Figure 2B**).

Identification of differentially expressed LncRNAs in HSVSMC treated with IL1α and PDGF

We next assessed whether lncRNAs were dynamically regulated by growth factor and cytokine stimulation. Approximately 33% of reads in each condition aligned to known or predicted lncRNAs (**Suppl. Figure 3A**). Differential expression analysis confirmed substantial differences in lncRNA expression between control and stimulated cells. Using the stringent criteria FDR ≤0.01 and log2 fold change (FC) ≥2, to declare significance and fragments per kilobase of exon per million fragments mapped (FPKM) >1, to confirm quantifiable expression we identified 224, 215 and 369 differentially expressed lncRNAs following IL1α, PDGF or dual stimulation respectively (**Suppl. Figure 3A**). Since lncRNAs can typically contain multiple splice variants, the numbers quoted refer to a single consensus gene model and therefore do not reflect the multiple transcripts of each lncRNA. To determine if specific biotypes of lncRNA were enriched following HSVSMC stimulation, those differentially expressed were further subdivided according to biotype in the Ensembl database. These are based upon their relative orientation to protein coding genes; intervening lncRNA (lincRNA), antisense, overlapping and processed transcripts. Utilising control and dual stimulation as an example, the distribution of different lncRNA biotypes was: intervening (45.5%), antisense (45.3%), overlapping (1.4%) and processed transcripts (7.9%) (**Suppl. Figure 3B).** Focusing on lincRNA, the candidates (control vs IL1α and PDGF, FDR<0.01, LogFC<2, FPKM>1) were ranked according to their FPKM and level of up/down-regulation (**Figure 2A, suppl Figure 4** for heat map of all conditions). A subset of the most differentially expressed transcripts was identified and validated by qRT–PCR (RP11-91k9.1, RP11-94a24.1, RP11-709B3.2, RP11-760H22.2 and AC018647.3; **Figure 2B**, chromosomal locations in **Suppl. Table. 1**). This was consistent with the RNA-seq results, showing RP11-94a24.1 and RP11-91k9.1upregulated 20.2±30and 45±26.4 fold, respectively following co-stimulation and lncRNAs RP11-709B3.2, RP11-760H22.2 and AC018647.3 being down regulated 16, 28 and 1209 fold, respectively (**Figure 3A**) (RQ = 0.06±0.04, 0.035±0.01 and 0.0008±0.001 respectively). The dissociation curves and gel products of each primer set are shown in **Supplemental Figure 5.**

Vascular enriched expression of RP11-94a24.1

The expression of each lncRNA was quantified in a range of 10 normal human tissues including specimens derived from brain, gastrointestinal, reproductive, and endocrine systems. In general, lncRNAs were expressed at relatively low levels across the tissue panel. However, we observed that RP11-91k9.1 was expressed highest in the heart, while RP11-91K9.1 and AC018647.3

showed preferential expression within the liver and brain respectively. RP11-709B3.2 and RP11-760H22.2 displayed highest expression in spleen and thyroid respectively (**Suppl. Figure 6A**). We next examined the expression of each lncRNA in primary HSVEC, HSVSMC and human coronary artery SMC (HCASMC). All lncRNAs had higher expression in VSMCs of either venous or arterial lineage compared to endothelial cells, suggesting VSMC enrichment (**Suppl. Figure 6B**). We also assessed whether the expression of these lncRNAs could be modulated by IL1α and PDGF in HSVEC as had been found in the HSVSMCs. Notably, subsequent down regulation of RP11-709B3.2, RP11-760H22.2 and AC018647.3 was not observed in HSVECs as was the case in HSVSMC (data not shown). Stimulation of HSVECs produced a significant 3.8±0.7 and 8.7±2.1 fold up regulation of RP11-91K9.1 following IL1α and IL1α/PDGF treatment respectively (**Figure 3B**). However, stimulation had no effect upon RP11-94a24.1 expression (**Figure 3B**), indicating selective regulation in HSVSMC. Due to the expression of RP11-94a24.1 in HSVSMC and its cell specific induction in response to pathological mediators of vascular injury, we focused further studies on RP11-94a24.1. We termed this lncRNA, smooth muscle induced lncRNA enhances replication (*SMILR*). *SMILR* expression was assessed through the utilisation of 3 independent primer sets targeting differential exons of the LncRNA. qRT-PCR revealed similar Ct and fold changes amongst the 3 sets, further confirming our previous data (Suppl. Figure 7). The longest open reading frame within *SMILR* is 57 amino acids. Analysis of this open reading frame using the Coding Potential Calculator (http://cpc.cbi.pku.edu.cn) did not reveal any similarity to known protein coding sequences suggesting that this RNA has no protein coding potential (data not shown).

IL1α/PDGF treatment induces the expression of SMILR in a time dependent manner

To investigate the longitudinal regulation of *SMILR*, we stimulated HSVSMC with PDGF, IL1α or a combination of both (1.5 h, 4 h, 24 h, 48 h and 72 h). We found significant up regulation of *SMILR* in response to PDGF as early as 4 h post stimulation. By 24 h *SMILR* expression was increased by treatment with PDGF or IL1α as well as both together (**Suppl. Figure 8**). The combination of PDGF and IL1α induced a synergistic increase in *SMILR* expression at 72 h.

Cellular localisation of SMILR in HSVSM cells

Rapid amplification of cDNA ends [25], was utilised to design specific RNA FISH probes. RNA-FISH highlighted a *SMILR* isoform, consisting of an additional 6bp at the 5' end and 316bp at the 3' end (**Suppl. Figure 9A and B**). RACE data is supported by the raw RNA-seq files (**Suppl. Figure 10 A-C**).

We performed RNA-FISH to provide visuospatial information as to the location of *SMILR* within HSVMSC. Negative control samples showed no fluorescent signal while SNORD3 fluorescent activity confirmed the nuclear permeabilisation of cells (**Figure 4A**). In the absence of growth factor and cytokine stimulation, HSVSMC typically exhibited between 0 and 3 positive fluorescent signals corresponding to *SMILR* localisation (**Figure 4A**). IL1α/PDGF treatment induced a marked increase in fluorescent signal within the nucleus and cytoplasm of HSVSMC. Further specificity of the FISH probes was confirmed through the utilisation of cells treated with either lentivirus containing *SMILR* or siRNA targeting *SMILR*. In each case an increase and decrease in *SMILR* transcripts was observed (**Figure 4A**). Quantification of FISH samples is provided in **Figure 4B**. In the absence of stimulation 2±3.6 SMILR molecules were observed. Following stimulation, 25±5 individual SMILR molecules were observed within the nucleus and cytoplasm (**Figure 4B**).

Identifying upstream mediators of SMILR expression in HSVSMC

It is well established that IL1α and PDGF work through distinct pathways leading to vascular cell activation. To assess the functional consequences of inhibition of these pathways on *SMILR* expression, selective pharmacological inhibitors AZD6244 (MEKK1) and SB 203580 (p38) were utilised (**Figure 5A**). Following 60 min pre-treatment with inhibitors, VSMC were stimulated with IL1α/PDGF and the expression of *SMILR* was determined at 24 h. Pre-treatment with AZD6244 (5, 10 or 15 µM) prevented the induction of *SMILR* in response to PDGF and IL1α (**Figure 5B**), while inhibition of p38 with SB203580 induced a dose-dependent reduction in *SMILR* expression in response to PDGF and IL1α (**Figure 5C**).

IL1α/PDGF treatment induces the release of SMILR into conditioned media

MicroRNAs have been reported to be secreted from cells as a means of cell to cell communication [26]. To investigate whether HSVSMCs release *SMILR* as an indication of expression, we modified a method commonly utilised to evaluate miRNA expression [27]. As no endogenous control was stably expressed across all conditions in this study, an exogenous control was added in order to monitor extraction efficiency and to normalise data. Consequently, total RNA from *C.elegans* was used as a spike-in and *ama-1* encoding polymerase II was chosen as a control for its high constitutive expression (see methods). Interestingly, *SMILR* was detected at low levels in media from quiesced VSMCs and those stimulated by either PDGF or IL1α, while conditioned media obtained from VSMC stimulated by combination contained significantly higher levels of *SMILR* (4.8±4.5 fold) (**Figure 5D**), consistent with the increased intracellular expression of *SMILR* following co-stimulation of VSMC. Thus, treatment with PDGF and IL1α increased intracellular and released levels of *SMILR*.

Additionally we sought to identify if *SMILR* was encapsulated within exosomes or microvesicles (MV). We utilised both ultracentrifugation, to remove cell debris, and an exosome isolation kit. **Supplemental Figure 11A and B** confirms the presence of microvesicles and exosomes using Nanosight technology and the expression of the previously described miR-143 within the exosomes/MV [28]. Our data highlights the expression of *SMILR* restricted to exosome free media (**Suppl. Figure 11C**) and inability to detect *SMILR* expression in the exosomes/MV compartment using both techniques of isolation. This observation has been confirmed by agarose gel electrophoresis (**Suppl. Figure 11D**). Primer melting curves are also shown in **Supplemental Figure 11E**. Our data confirm that *SMILR* is secreted into the media and located in a non-exosome/MV fraction. This could possibly be through interaction with specific membrane channels but requires additional experimentation.

Additionally, we examined the release of *SMILR* following lentiviral overexpression in IL1 and PDGF treated cells. Lentiviral overexpression resulted in a 10-fold increase in *SMILR* RNA intracellularly. However, only a marginal (not significant) increase was observed within conditioned media analysed from infected cells (**Suppl. Figure 11F**). When this media was transferred onto additional quiesced cells, no change in proliferation was detected (**Suppl. Figure 11G**). This may suggest that the release of *SMILR* is under stringent control mechanism and simply increasing *SMILR* expression via lentiviral approach is not sufficient to induce the additional release of this lncRNA from the cells. In addition, these cells were stimulated with IL1 and PDGF, which strongly enhances *SMILR* expression in VSMC. The secretory machinery may have been saturated with the high levels of LncRNA within the cytoplasm. This has previously been demonstrated with microRNA where high levels of miR, via overexpression with microRNA mimics, saturated the exportin-5 pathway of endogenous miRNAs with fatal consequences[29, 30].

Effect of dicer substrate siRNA mediated knockdown of SMILR on HSVSMC proliferation

We investigated the function of *SMILR* using dicer substrate siRNA (dsiRNA)-mediated knockdown and EdU incorporation. Forty-eight hours post stimulation, IL1 and PDGF treatment induced a 34±15% increase in VSMC proliferation compared to control (**Suppl. Figure 12**). DsiRNA *SMILR* caused 75±24% decrease in *SMILR* expression when compared to dsiControl (**Figure 5E**). Following *SMILR* knock down with dsiRNA, VSMC proliferation was reduced by 56±15% (**Figure 5F**). Results were confirmed through the use of a second dsiRNA targeting an alternative region of *SMILR* (**Suppl. Figure 13A and B**). No effect on the interferon pathway was observed upon assessment of the response genes *OAS1* and *IRF7*, which have previously been linked to disRNA off target effects [31] (**Suppl. Figure 13C and D**).

Additionally the effect of *SMILR* overexpression on SMC proliferation was investigated. SMC were infected with *SMILR* lentivirus or empty control for 24 hours prior to stimulation. Infection at a multiplicity of infection of 25 and 50 produced a 5.5 ± 3.5 and 11.4 ± 4.7 fold increase in *SMILR* expression compared to the empty control, with no apparent toxicity effects (**Figure 5G**). Overexpression produced a dose dependent increase of 1.3 ± 0.3 fold and 1.66 ± 0.5 fold in SMC proliferation respectively (**Figure 5H**), confirming the knock down data.

SMILR expression correlates with other proximal genes

The expression of lincRNAs can correlate with the expression of adjacent genes and other RNAs within the genomic locale [32]. We therefore assessed the expression of genes and non-coding RNAs within 5 million base pairs of *SMILR*, from *COL14A1* on the forward strand to *FERIL6-AS1* on the reverse strand (**Figure 6A**), using the RNA-seq data set (**Figure 6B**). Up-regulation of *SMILR* was not associated with a widespread increase in transcriptional activity within the region (**Figure 6B**). However, similar changes in expression in response to VSMC stimulation were observed in two proximal transcripts (*HAS2* and *HAS2-AS1*). *SMILR* is located ~750 kbp downstream of *HAS2* on the same (reverse) strand and ~350 kbp from *ZHX2* and ~ 750 kbp from

HAS2-AS1 on the opposite strand of chromosome 8 (**Figure 6C**). The upregulation of HAS2 was accompanied by an increase in HAS1 but not HAS3 following dual stimulation (**Figure 6 D-F***)*. Interestingly, IL1 and PDGF in combination had no effect on HAS3 expression as IL1 and PDGF have opposing effects on HAS3 expression (Full graph with single stimulation **Suppl. Figure 13 E and F**). In addition to *SMILR*, up-regulation of *HAS2-AS1* was evident following IL1α and PDGF treatment, but not *ZHX1* in the RNA-seq data (*Data not shown).* This observation was validated by qRT-PCR (**Figure 6 G,H and I***)*.

It has been previously shown that lncRNA can modulate the expression of nearby protein coding genes. Thus, the expression of proximal genes *HAS2*, *ZHX2* and *HAS2-AS1* were determined following *SMILR* knockdown. RNAi-mediated knockdown of *SMILR* significantly altered levels of *HAS2* mRNA. However, no change in the *HAS2-AS1* lncRNA or the *ZHX2* gene was observed via qRT-PCR (**Figure 6 J-L**). Results were confirmed using a second siRNA targeting *SMILR* (**Suppl. Figure 13 G - I**). Additionally, no effect on HAS1 or HAS3 expression was observed while utilising *SMILR* siRNA indicating that the effect of *SMILR* knockdown is specific to HAS2 and not all isoforms of HAS (**Figure 6 M and N**).

Additionally, knockdown of HAS2-AS1 greatly reduced HAS2 expression with no effect on *SMILR* expression (**Suppl. Figure 14 A and 14B**). However, the reverse experiment utilising HAS2 knockdown, did not affect the expression of HAS2-AS1 nor *SMILR* (**Suppl. Figure 14C**). Finally, lentiviral mediated overexpression did not affect HAS1, 2,3 or HAS2-AS1 expression (**Suppl. Figure 14 D-G**).

SMILR expression is dysregulated in unstable human carotid plaques

To investigate the importance of *SMILR* in human vascular pathologies, we assessed levels of *SMILR* in unstable atherosclerotic plaques. We used two established inflammatory ([18F]-

fluorodeoxyglucose (FDG) and calcification ([18F]-fluoride) PET radiotracers to define prospectively portions of high-risk plaque [33] [34] [35] for RNA extraction. Plaque and relatively 'healthy' adjacent sections of vessel were assessed from within individual patients (**Suppl. Table 5** for patient characteristics). This is of key importance as it permits the assessment of non-coding RNA expression from within each micro environment (plaque vs. non plaque) from within the one vessel. Compared to quiescent adjacent tissue, portions of high-risk plaque showed higher uptake of both [18F]-FDG (maximum tissue-to-background ratio (TBR_{max}) 1.81±0.21 *versus* 1.31±1.6) and [18F]-fluoride (TBR_{max} 2.32±0.52 *versus* 1.31±0.43) indicating that plaques subjected to RNA analysis had enhanced rates of inflammation (**Figure 7A-G** for image examples and **Figure 7 H-K** for graphs of tracer uptake). Since non-coding RNAs have not been assessed in a similar sample set before, we first confirmed whether expression of a panel of miRNAs associated with atherosclerosis processes were dysregulated [36]. As expected, inflammation-associated miRNAs 146a-and 146b were significantly upregulated in unstable plaques compared to adjacent quiescent tissue, while miR-29 and miR-204, which are inversely associated with osteoblastogenesis and arterial calcification, were down regulated in mineralised regions of the atherosclerotic plaque [37, 38]. In addition we also found a downregulation of the miR-143/145 cluster, which is associated with SMC differentiation and aortic aneurysm formation [39], an event which has previously been linked to osteogenic differentiation of SMC (**Figure 7L**). Thus expression of small non-coding RNAs (miRs) was associated with PET/CT defined high-risk plaques. Therefore, we utilised the same cohort of samples to assess *SMILR*, *HAS2* and *HAS2-AS1* levels. A 3.9±2.3 fold increase in *SMILR* expression was observed in high-risk plaques compared to adjacent stable regions of the carotid artery (**Figure 7M**). Intriguingly, we also observed an increased in HAS2 (**Figure 7N**) but not *HAS2-AS1* (**Figure 7O**).

SMILR is detectable in human plasma and correlates with inflammatory CRR

Due to the release of *SMILR* into conditioned media from VSMC following stimulation with inflammatory mediators, we evaluated whether *SMILR* was detectable in stored samples from a cohort of men with varying metabolic dysfunction. These samples were ranked in order of the serologic parameter CRP levels into 3 groups: CRP <2, CRP 2-5 and CRP >5 mg/L representing broad tertiles of CRP. *SMILR* showed no difference in patients with CRP levels below 2 mg versus 2-5 mg/L. However, a 3.3±5.7 fold increase in *SMILR* was observed when CRP concentrations were greater than 5 mg/L (**Figure 8A**). Furthermore, a significant positive correlation was seen between *SMILR* and CRP (R^2=0.33, P<0.0001) (**Figure 8B**). There was no correlation between *SMILR* and additional risk factors including age (P=0.66), blood pressure (P=0.12), BMI (P=0.14) or social deprivation status (P=0.11) (**Suppl. Table 6**). Melting curves and gel products of *SMILR* primers in plasma are shown in **Supplemental Figure 15**. Further information regarding the statistical analysis of *SMILR* CRP correlation can be found in **Supplemental Figure 16**.

Discussion

We have shown that stimulation of HSVSMCs with PDGF and IL1α increases expression of *SMILR*. This novel lincRNA increases cell proliferation which may be linked to its ability to regulate the proximal gene *HAS2*. In a clinical setting, we found increased expression of *SMILR* in unstable atherosclerotic plaques suggesting an association with fundamentally important vascular pathologies linked to inflammation and VSMC proliferation. We also discovered that *SMILR* can be released from cells and is detectable in plasma from patients with enhanced inflammation and thus susceptibility to atherosclerosis. These findings support the growing body of evidence that non-coding RNAs can act as mediators to modulate disease pathways.

Recent advances in RNA-sequencing have demonstrated that previously thought "genome deserts" are in fact pervasively transcribed and are populated by lncRNAs. Utilising paired end-sequencing allowed accurate alignment of reads to the human genome (GRCh37), the 93% alignment rate met quality standards for the RNA-seq technique [40] and ensured that our RNA-seq provided a high quality profile of the HSVSMC transcriptome during quiescent and stimulated conditions. Notably, compared to control cells, protein-coding genes accounted for 3-4 fold greater abundance than lncRNAs. Our RNA-seq depth of 70 million reads was sufficient to identify lncRNAs within VSMC, however, it should be noted that greater read depths and use of refined capture-seq technique would be beneficial in order to offer greater annotation of specific areas within the genome.

Analysis of the RNA-seq data pinpointed *SMILR* as an IL1α/PDGF responsive lincRNA located on chromosome 8, 750 kbp from the closest protein-coding gene, on the same strand. This gene, *HAS2*, encodes an enzyme which synthesises hyaluronic acid (HA), a critical component of the extracellular matrix that accumulates in human restenotic and atherosclerotic lesions [41, 42]. Our results show knockdown of *SMILR* reduces *HAS2* expression and VSMC proliferation. This mechanism of action is supported by a number of studies demonstrating HA can enhance VSMC proliferation and migration [43]. Recent studies using transgenic mice with VSMC specific over-expression of HA have found increased susceptibility to atherosclerosis [44] and enhanced neointima formation in response to cuff injury [45]. The ability of *SMILR* to specifically target HAS2 with no effect on HAS1 or HAS3 allows a means of specifically altering HAS2 expression, the main HAS isoform expressed and functioning in SMC pathology[46].

LncRNAs can regulate other RNAs via a number of mechanisms [47], including changes in chromatin signatures within their locus. For example, the *HOTAIR* lncRNA is capable of repressing transcription in trans across 40 kbp of the HOXD locus [48]. Thus *SMILR* may act as an enhancer or scaffold via interaction with the promoter region, and potentially other transcription factors of *HAS2*, to regulate expression following inflammatory cytokine stimulation. However, further detailed co-immunoprecipitation or site directed mutagenesis studies would be required to demonstrate whether *SMILR* participates in transcription factor complexes with NF-κβ or other transcription factors. Previous work has found *HAS2* is regulated by an additional lncRNA, *HAS2-AS1* [49]. Interestingly, our RNA-seq data show *HAS2-AS1* expression was also upregulated by PDGF treatment alone and in combination with IL1α. However, knockdown of *SMILR* did not alter *HAS2-AS1* expression. LncRNA *HAS2-AS1* modulates chromatin structures around the gene in order to allow more efficient binding of the RNA polymerase 2, and enhance *HAS2* gene expression[49]. This suggests both *SMILR* and *HAS2-AS1* can regulate *HAS2* by independent mechanisms. Interestingly, knockdown of HAS2 did not affect either *SMILR* nor HAS2-AS1 expression indicating that the expression of these lncRNA are not directly linked to HAS2 expression.

The composition of ECM assists in the determination of the stability of the atherosclerotic plaques, the phenotype of cells within it and the volume of neointima. During the progression of atherosclerosis, VSMC are exposed to a plethora of signalling molecules, including inflammatory cytokines. Using the clinical gold-standard methods of 18F-FDG and 18F-fluoride PET/CT imaging to identify inflamed, necrotic and mineralising atherosclerotic plaque [33 34], our results indicate miRs 29, 143, 145, 146 and 204 are differentially expressed in unstable regions of atherosclerotic plaques. These miRs have previously been linked to VSMC differentiation, inflammatory cell signalling [50] and VSMC calcification [51]. The strong association and co-localisation of *SMILR* with this classical miRNA profile and focal 18F-FDG and 18F-fluoride uptake within atherosclerotic plaque suggests that *SMILR* may play a role in atherosclerosis through inflammatory and proliferative pathways. In keeping with our results showing *HAS2* regulation by *SMILR*, HA content has been shown to reflect the progression of atherosclerotic disease and promotes vessel wall thickening[52]. Indeed, HA has been implicated in the recruitment of inflammatory cells, known to play a prominent role in the initiation and progression of atherosclerotic lesion to an unstable plaque phenotype.

Our results demonstrate *SMILR* is up-regulated by a combination of PDGF and IL1α in VSMCs but not ECs, suggesting modulation of *SMILR* could specifically alter VSMC proliferation without detrimental effects on vessel re-endothelialisation. If this is the case, it would provide a suitable candidate to improve current anti-proliferative therapies since current pharmacological agents target cell proliferation in a non-cell specific manner, events which can lead to late stent thrombosis [53].

The ability to identify confidently a plaque, or patient, at particular risk of a major adverse cardiovascular event (i.e plaque rupture) remains an important goal of Cardiovasc Res. Long RNA, both mRNA and non-coding RNA, have been previously shown to be stable in vivo for up to 3 weeks [54]. As such the search for prognostic biomarkers has greatly increased in recent years. *SMILR* was expressed in both the nucleus and cytoplasm of cells following stimulation and was released into the media. It will be important to determine whether the cytoplasmic copies induce functional effects, such as regulation of gene expression through post-translational mechanisms or if they are simply being processed for release. Dual transcriptional functions of lncRNAs have been shown previously[55], but to date no reports of a single lncRNA affecting both transcription and translation have been published. The release of *SMILR* could affect function in neighbouring cells, particularly in a vascular injury setting where phenotypic switching of VSMCs occurs in distinct areas of the vessel wall. In support of this theory, it has been shown that miR 143/145 can be transferred from VSMC into EC[56]. This transfer produced physiological effects within EC including modulation of angiogenesis. We also found that *SMILR* could be detected in the plasma of patients with higher CRP levels indicative of chronic low grade inflammation. In light of our studies, we propose this release could be due to the increased levels of *SMILR* in the diseased vasculature, although delineating whether plasma *SMILR* is simply a by-product of increased intracellular levels or is functionally active in disease pathology is difficult to definitely demonstrate. However, circulating levels of miR 143 and 145 are associated with in-stent restenosis and as such have been proposed as biomarkers[57]. The correlation of *SMILR* and high CRP further supports its expression in low grade chronic inflammatory settings as well as proliferative settings. Further large clinical cohorts will be required to ascertain if *SMILR* has prognostic potential in inflammatory vascular disease, and if so, whether it provides enhanced prognostic value over current biomarkers.

Vessel re-narrowing after surgical intervention and atherosclerosis remain significant clinical problems and HA/*HAS2*/*SMILR* have emerged as key components of these pathological processes. Administration of an siRNA targeting *SMILR* could be used to prevent re-narrowing after surgical intervention for acute coronary syndrome. Using siRNAs has been proven to be effective in phase I clinical trials. *Davis et al*. recently showed a dose-dependent increase of siRNA delivered via nanoparticles and observed a reduction in the specific mRNA target[58]. However, we must remain cautious, since early clinical trials in the setting of vein graft failure suggested that antisense oligonucleotides directed again E2F (edifoligide) held promising for the treatment of vein graft failure and atherosclerosis, but the subsequent phase-three PREVENT IV study yielded largely disappointing results [59]. However, these studies do demonstrate that the surgical setting of coronary artery bypass grafting provides the ideal clinical setting to evaluate the clinical efficacy of these targets by gene therapy, given that the vein can be transduced *ex vivo* at the time of surgery Administration of siRNA directly to the vessel would obviate the need to administer siRNA systemically and thus reduce the possibility of off target effects. Unfortunately, there are no clear homologues of *SMILR* in the mouse. It would, however, be important to determine if other pre-clinical models of human vascular disease contain *SMILR* homologues, once this information becomes available.

Taken together, these observations broaden our awareness of the complex interplay between lncRNA and protein coding genes. The emergence of lncRNAs as regulators of gene expression will undoubtedly alter our understanding of the complex regulation network of pathological VSMC proliferation in vascular disease and may provide a means to specifically target VSMC or identify patients at risk of major adverse vascular outcomes.

Acknowledgments: We thank N. Britton and G. Aitchison for technical assistance.

Funding Sources: This work is supported by the British Heart Foundation (Programme grant: RG/09/005/27915 and FS11/12/28673). MDB is supported by the British Heart Foundation PhD Studentship (FS/12/66/30003) and AHB is supported by the British Heart Foundation Chair of Translational Cardiovascular Sciences (CH/11/2/28733). Clinical PET/CT studies and AV were funded by the British Heart Foundation (PG/12/8/29371). MRD and DEN are supported by the British Heart Foundation (FS/14/78/31020 and CH/09/002). DEN is the recipient of a Wellcome Trust Senior Investigator Award (WT103782AIA). The Wellcome Trust Clinical Research Facility and the Clinical Research Imaging Centre are supported by NHS Research Scotland (NRS) through NHS Lothian.

Conflict of Interest Disclosures: None.

References:

1. Marx SO, Totary-Jain H, Marks AR. Vascular smooth muscle cell proliferation in restenosis. *Circ Cardiovasc Interv*. 2011;4:104-111.

2. Ghouri N, Purves D, McConnachie A, Wilson J, Gill JM, Sattar N. Lower cardiorespiratory fitness contributes to increased insulin resistance and fasting glycaemia in middle-aged South Asian compared with European men living in the UK. *Diabetologia*. 2013;56:2238-2249.

3. Gomez D, Owens GK. Smooth muscle cell phenotypic switching in atherosclerosis. *Cardiovasc Res*. 2012;95:156-164.

4. Alexander MR, Owens GK. Epigenetic control of smooth muscle cell differentiation and phenotypic switching in vascular development and disease. *Ann Rev Physiol.* 2012;74:13-40.

5. Schermuly RT, Dony E, Ghofrani HA, Pullamsetti S, Savai R, Roth M, Sydykov A, Lai YJ, Weissmann N, Seeger W, Grimminger F. Reversal of experimental pulmonary hypertension by PDGF inhibition. *J Clin Invest.* 2005;115:2811-2821.

6. Rectenwald JE, Moldawer LL, Huber TS, Seeger JM, Ozaki CK. Direct evidence for cytokine involvement in neointimal hyperplasia. *Circulation*. 2000;102:1697-1702.

7. Dardik A, Yamashita A, Aziz F, Asada H, Sumpio BE. Shear stress-stimulated endothelial cells induce smooth muscle cell chemotaxis via platelet-derived growth factor-BB and interleukin-1alpha. *J Vasc Surg*. 2005;41:321-331.

8. Ferns GA, Raines EW, Sprugel KH, Motani AS, Reidy MA, Ross R. Inhibition of neointimal smooth muscle accumulation after angioplasty by an antibody to PDGF. *Science*. 1991;253:1129-1132.

9. Guan S, Tang Q, Liu W, Zhu R, Li B. Nobiletin Inhibits PDGF-BB-induced vascular smooth muscle cell proliferation and migration and attenuates neointimal hyperplasia in a rat carotid artery injury model. *Drug Dev Res*. 2014;75:489-496.

10. Johnson JL, Dwivedi A, Somerville M, George SJ, Newby AC. Matrix metalloproteinase (MMP)-3 activates MMP-9 mediated vascular smooth muscle cell migration and neointima formation in mice. *Arterioscler Thromb Vasc Biol.* 2011;31:e35-44.

11. Elgar G, Vavouri T. Tuning in to the signals: noncoding sequence conservation in vertebrate genomes. *Trends Genet*. 2008;24:344-352.

12. Salic K, De Windt LJ. MicroRNAs as biomarkers for myocardial infarction. *Curr Atheroscler Rep.* 2012;14:193-200.

13. Jiang Y, Wang HY, Li Y, Guo SH, Zhang L, Cai JH. Peripheral blood miRNAs as a biomarker for chronic cardiovascular diseases. *Sci Rep*. 2014;4:5026.

14. Jiang Y, Wang HY, Cao HM, Wang CY, Zhang L, Wang H, Liu L, Li Y, Cai JH. Peripheral blood miRNAs as a biomarker for chronic cardiovascular diseases. *Sci Rep*. 2014;4.

15. Kaushik K, Leonard VE, Kv S, Lalwani MK, Jalali S, Patowary A, Joshi A, Scaria V, Sivasubbu S. Dynamic expression of long non-coding RNAs (lncRNAs) in adult zebrafish. *PloS one*. 2013;8:e83616.

16. Liu JY, Yao J, Li XM, Song YC, Wang XQ, Li YJ, Yan B, Jiang Q. Pathogenic role of lncRNA-MALAT1 in endothelial cell dysfunction in diabetes mellitus. *Cell Death Dis.* 2014;5:e1506.

17. Bell RD, Long X, Lin M, Bergmann JH, Nanda V, Cowan SL, Zhou Q, Han Y, Spector DL, Zheng D, Miano JM. Identification and initial functional characterization of a human vascular cell-enriched long noncoding RNA. *Arterioscler Thromb Vasc Biol.* 2014;34:1249-1259.

18. Jaffe EA, Nachman RL, Becker CG, Minick CR. Culture of human endothelial cells derived from umbilical veins. Identification by morphologic and immunologic criteria. *J Clin Invest.* 1973;52:2745-2756.

19. Southgate KM, Davies M, Booth RF, Newby AC. Involvement of extracellular-matrix-degrading metalloproteinases in rabbit aortic smooth-muscle cell proliferation. *Biochem J.* 1992;288 (Pt 1):93-9.

20. Dodt M, Roehr JT, Ahmed R, Dieterich C. FLEXBAR-Flexible Barcode and Adapter Processing for Next-Generation Sequencing Platforms. *Biology*. 2012;1:895-905.

21. Kim D, Pertea G, Trapnell C, Pimentel H, Kelley R, Salzberg SL. TopHat2: accurate alignment of transcriptomes in the presence of insertions, deletions and gene fusions. *Genome Biol.* 2013;14:R36.

22. Trapnell C, Williams BA, Pertea G, Mortazavi A, Kwan G, van Baren MJ, Salzberg SL, Wold BJ, Pachter L. Transcript assembly and quantification by RNA-Seq reveals unannotated transcripts and isoform switching during cell differentiation. *Nat Biotechnol.* 2010;28:511-515.

23. Trapnell C, Hendrickson DG, Sauvageau M., Goff L, Rinn JL, Pachter L. Differential analysis of gene regulation at transcript resolution with RNA-seq. *Nat Biotechnol.* 2012;1:46-53.

24. Livak KJ, Schmittgen TD. Analysis of relative gene expression data using real-time quantitative PCR and the 2(-Delta Delta C(T)) Method. *Methods*. 2001;25:402-408.

25. Billings FTt, Balaguer JM, C Y, Wright P, Petracek MR, Byrne JG, Brown NJ, Pretorius M. Comparative effects of angiotensin receptor blockade and ACE inhibition on the fibrinolytic and inflammatory responses to cardiopulmonary bypass. *Clin Pharmacol Ther*. 2012;91:1065-1073.

26. Glynn CL, Khan S, Kerin MJ, Dwyer RM. Isolation of secreted microRNAs (miRNAs) from cell-conditioned media. *MicroRNA*. 2013;2:14-19.

27. Morley-Smith AC, Mills A, Jacobs S, Meyns B, Rega F, Simon AR, Pepper JR, Lyon AR, Thum T. Circulating microRNAs for predicting and monitoring response to mechanical circulatory support from a left ventricular assist device. *Eur J Heart Fail*. 2014;16:871-879.

28. Deng L, Blanco FJ, Stevens H, Lu R, Caudrillier A, McBride M, McClure JD, Grant J, Thomas M, Frid M, Stenmark K, White K, Seto AG, Morrell NW, Bradshaw AC, MacLean MR, Baker AH. MicroRNA-143 Activation Regulates Smooth Muscle and Endothelial Cell Crosstalk in Pulmonary Arterial Hypertension. *Circ Res*. 2015;117:870-883.

29. Soifer HS, Rossi JJ, Saetrom P. MicroRNAs in disease and potential therapeutic applications. *Mol Ther*. 2007;15:2070-2079.

30. Grimm D, Streetz KL, Jopling CL, Storm TA, Pandey K, Davis CR, Marion P, Salazar F, Kay MA. Fatality in mice due to oversaturation of cellular microRNA/short hairpin RNA pathways. *Nature*. 2006;441:537-541.

31. Karpala AJ, Doran TJ, Bean AG. Immune responses to dsRNA: implications for gene silencing technologies. *Immunol Cell Biol*. 2005;83:211-216.

32. Wang KC, Chang HY. Molecular mechanisms of long noncoding RNAs. *Mol Cell*. 2011;43:904-914.

33. Rudd JH, Warburton EA, Fryer TD, Jones HA, Clark JC, Antoun N, Johnstrom P, Davenport AP, Kirkpatrick PJ, Arch BN, Pickard JD, Weissberg PL. Imaging atherosclerotic plaque inflammation with [18F]-fluorodeoxyglucose positron emission tomography. *Circulation*. 2002;105:2708-2711.

34. Joshi NV, Vesey AT, Williams MC, Shah AS, Calvert PA, Craighead FH, Yeoh SE, Wallace W, Salter D, Fletcher AM, van Beek EJ, Flapan AD, Uren NG, Behan MW, Cruden NL, Mills NL, Fox KA, Rudd JH, Dweck MR, Newby DE. 18F-fluoride positron emission tomography for identification of ruptured and high-risk coronary atherosclerotic plaques: a prospective clinical trial. *Lancet*. 2014;383:705-713.

35. Vesey AT, Irkle A, Lewis DY, Skepper JN, Bird JLE, Dweck MR, Joshi FR, Gallagher FA, Warburton EA, Bennett MR, Brindle KM, Newby DE, Rudd JH, Davenport AP. YY Identifying Active Vascular Microcalcification By F-18-Sodium Fluoride Positron Emission Tomography. *Brit J Surg*. 2015;102:5-5.

36. Raitoharju E, Lyytikainen LP, Levula M, Oksala N, Mennander A, Tarkka M, Klopp N, Illig T, Kahonen M, Karhunen PJ, Laaksonen R, Lehtimaki T. miR-21, miR-210, miR-34a, and miR-146a/b are up-regulated in human atherosclerotic plaques in the Tampere Vascular Study. *Atherosclerosis*. 2011;219:211-217.

37. Du Y, Gao C, Liu Z, Wang L, Liu B, He F, Zhang T, Wang Y, Wang X, Xu M, Luo GZ, Zhu Y, Xu Q, Wang X, Kong W. Upregulation of a disintegrin and metalloproteinase with thrombospondin motifs-7 by miR-29 repression mediates vascular smooth muscle calcification. *Arterioscler Thromb Vasc Biol.* 2012;32:2580-2588.

38. Cui RR, Li SJ, Liu LJ, Yi L, Liang QH, Zhu X, Liu GY, Liu Y, Wu SS, Liao XB, Yuan LQ, Mao DA, Liao EY. MicroRNA-204 regulates vascular smooth muscle cell calcification in vitro and in vivo. *Cardiovasc Res*. 2012;96:320-329.

39. Elia L, Quintavalle M, Zhang J, Contu R, Cossu L, Latronico MV, Peterson KL, Indolfi C, Catalucci D, Chen J, Courtneidge SA, Condorelli G. The knockout of miR-143 and -145 alters smooth muscle cell maintenance and vascular homeostasis in mice: correlates with human disease. *Cell Death Differ*. 2009;16:1590-1598.

40. Mortazavi A, Williams BA, McCue K, Schaeffer L, Wold B. Mapping and quantifying mammalian transcriptomes by RNA-Seq. *Nat Methods*. 2008;5:621-628.

41. Papakonstantinou E, Roth M, Block LH, Mirtsou-Fidani V, Argiriadis P, Karakiulakis G. The differential distribution of hyaluronic acid in the layers of human atheromatic aortas is associated with vascular smooth muscle cell proliferation and migration. *Atherosclerosis*. 1998;138:79-89.

42. Riessen R, Wight TN, Pastore C, Henley C, Isner JM. Distribution of hyaluronan during extracellular matrix remodeling in human restenotic arteries and balloon-injured rat carotid arteries. *Circulation*. 1996;93:1141-1147.

43. Papakonstantinou E, Karakiulakis G, Roth M, Block LH. Platelet-derived growth factor stimulates the secretion of hyaluronic acid by proliferating human vascular smooth muscle cells. *Proc Natl Acad Sci U S A*. 1995;92:9881-9885.

44. Chai S, Chai Q, Danielsen CC, Hjorth P, Nyengaard JR, Ledet T, Yamaguchi Y, Rasmussen LM, Wogensen L. Overexpression of hyaluronan in the tunica media promotes the development of atherosclerosis. *Circ Res*. 2005;96:583-591.

45. Kashima Y, Takahashi M, Shiba Y, Itano N, Izawa A, Koyama J, Nakayama J, Taniguchi S, Kimata K, Ikeda U. Crucial role of hyaluronan in neointimal formation after vascular injury. *PloS one*. 2013;8:e58760.

46. van den Boom M, Sarbia M, von Wnuck Lipinski K, Mann P, Meyer-Kirchrath J, Rauch BH, Grabitz K, Levkau B, Schror K and Fischer JW. Differential regulation of hyaluronic acid synthase isoforms in human saphenous vein smooth muscle cells: possible implications for vein graft stenosis. *Circ Res*. 2006;98:36-44.

47. Geisler S, Coller J. RNA in unexpected places: long non-coding RNA functions in diverse cellular contexts. *Nat Rev Mol Cell Biol*. 2013;14:699-712.

48. Rinn JL, Kertesz M, Wang JK, Squazzo SL, Xu X, Brugmann SA, Goodnough LH, Helms JA, Farnham PJ, Segal E, Chang HY. Functional demarcation of active and silent chromatin domains in human HOX loci by noncoding RNAs. *Cell*. 2007;129:1311-1123.

49. Vigetti D, Deleonibus S, Moretto P, Bowen T, Fischer JW, Grandoch M, Oberhuber A, Love DC, Hanover JA, Cinquetti R, Karousou E, Viola M, D'Angelo ML, Hascall VC, De Luca G, Passi A. Natural antisense transcript for hyaluronan synthase 2 (HAS2-AS1) induces transcription of HAS2 via protein O-GlcNAcylation. *J Biol Chem*. 2014;289:28816-28826.

50. Taganov KD, Boldin MP, Chang KJ, Baltimore D. NF-kappaB-dependent induction of microRNA miR-146, an inhibitor targeted to signaling proteins of innate immune responses. *Proc Natl Acad Sci U S A*. 2006;103:12481-12486.

51. Du Y, Gao C, Liu Z, Wang L, Liu B, He F, Zhang T, Wang Y, Wang X, Xu M, Luo GZ, Zhu Y, Xu Q, Kong W. Upregulation of a disintegrin and metalloproteinase with thrombospondin motifs-7 by miR-29 repression mediates vascular smooth muscle calcification. *Arterioscler Thromb Vasc Biol*. 2012;32:2580-2588.

52. Johnson JL. Matrix metalloproteinases: influence on smooth muscle cells and atherosclerotic plaque stability. *Expert Rev Cardiovasc Ther*. 2007;5:265-282.

53. Lemesle G, Maluenda G, Collins SD, Waksman R. Drug-eluting stents: issues of late stent thrombosis. *Cardiol Clin*. 2010;28:97-105.

54. Pinel K, Lacoste J, Plane G, Ventura M, Couillaud F. Long-term in vivo imaging of translated RNAs for gene therapy. *Gene Ther*. 2014;21:434-439.

55. Vance KW, Sansom SN, Lee S, Chalei V, Kong L, Cooper SE, Oliver PL, Ponting CP. The long non-coding RNA Paupar regulates the expression of both local and distal genes. *EMBO J*. 2014;33:296-311.

56. Climent M, Quintavalle M, Miragoli M, Chen J, Condorelli G, Elia L. TGFbeta Triggers miR-143/145 Transfer From Smooth Muscle Cells to Endothelial Cells, Thereby Modulating Vessel Stabilization. *Circ Res*. 2015;116:1753-1764.

57. He M, Gong Y, Shi J, Pan Z, Zou H, Sun D, Tu X, Tan X, Li J, Li W, Liu B, Xue J, Sheng L, Xiu C, Yang N, Xue H, Ding X, Yu C, Li Y. Plasma microRNAs as potential noninvasive biomarkers for in-stent restenosis. *PloS one*. 2014;9:e112043.

58. Davis ME, Zuckerman JE, Choi CH, Seligson D, Tolcher A, Alabi CA, Yen Y, Heidel JD, Ribas A. Evidence of RNAi in humans from systemically administered siRNA via targeted nanoparticles. *Nature*. 2010;464:1067-1070.

59. Hess CN, Lopes RD, Gibson CM, Hager R, Wojdyla DM, Englum BR, Mack MJ, Califf RM, Kouchoukos NT, Peterson ED, Alexander JH. Saphenous vein graft failure after coronary artery bypass surgery: insights from PREVENT IV. *Circulation*. 2014;130:1445-1451.

Clinical Perspective

Long noncoding RNAs (lncRNAs) are a relatively new class of discovered RNA molecules that possess important regulatory functions. The rapidly expanding catalogue of lncRNAs holds promise that in the near future lncRNAs might become relevant to vascular disease clinically, as possible biomarkers of cardiovascular events and for targeted treatment of disease. Our work indicates that dysregulation of key lncRNAs may have profound implications in regulating vascular smooth muscle cell function. In addition, we detected the release of this lncRNA in plasma samples and correlated with inflammatory CReactive Protein (CRP) levels, highlighting new methods and possibilities for improved detection. The emergence of lncRNAs as regulators of gene expression and vascular function will undoubtedly alter our understanding of the complex regulation network of cell function underpinning clinical vascular disease.

Figure Legends:

Figure 1. RNA sequencing shows IL1α and PDGF induction of inflammatory and cell cycle pathways. (A): Study design for determination of the transcriptome in quiescent and stimulated HSVSMC. HSVSMC were treated for 72 h, RNA quality assessed and subjected to RNA-seq following the Tuxedo pipeline for analysis. (B): Known inflammatory microRNA, miR146a, is upregulated by IL1α (n=4). **P<0.01 vs. 0.2% condition. Multiple comparison one-way ANOVA. (C): BrdU incorporation as an indirect marker of proliferation was assessed in all patients. (n=3). **P<0.01 vs. 0.2% condition. (D): Biotype distribution of all transcripts identified by RNA-seq analysis generated from HSVSM cells treated with IL1α and PDGF, cutoff at FPKM>0.1 (E): Venn diagram indicating overlap of protein coding genes with altered expression (analysed using EdgeR, FDR<0.01) across each treatment.

Figure 2. Identification of differentially expressed LncRNAs in HSVSMC treated with IL1α and PDGF. (**A**): Heatmaps showing order of differentially expressed transcripts within the 4 patient samples before and after IL1α/PDGF treatment. LncRNA selected for validation marked by * (**B**): Heatmap representing the fold change of the 5 lncRNAs selected for validation. Heatmaps represent data from RNA-seq pipeline.

Figure 3. Treatment with IL1α and PDGF significantly altered LncRNA expression and showed distinct expression within vascular cell types. (A): Graphs indicate fold change of lncRNA from RNA-seq data and subsequent validation by qRT-PCR (*n=4*). * P<0.05, ** P<0.01, *** P<0.001 vs 0.2% condition. (B): Basal and stimulated expression of lncRNAs 2 and 7 within HSVEC and

HSVSMC (*n=4 for SMC and n=3 for EC*, * P<0.05, ** P<0.01, *** P<0.001 vs 0.2% in each specific cell type).

Figure 4. Localisation of *SMILER*. (A): RNA FISH analysis of *SMILR,* cytoplasmic *UBC* mRNA and nuclear *SNORD3* RNA in HSVSMC, Magnification x630 for all panels. UBC and SNORD3 used for confirmation of cellular compartments (B): Quantification of LncRNA molecules per cell in indicated conditions. Greater than 5 images were selected at random from each condition and at least 4 cells counted in each image.

Figure 5. Functional regulation of *SMILR*. (A): Schematic diagram showing specific sites of inhibition. HSVSMC were pre-treated for 60minutes with the indicated concentration of the inhibitors. Following exposure to vehicle or 10ng/ml IL1 or 20nM PDGF for 24 h expression of SMILR was determined by qRT-PCR. (B): SMILR expression following MEKK1 inhibition. ***P<0.01 vs 0.2% media, ### P<0.001 vs IL1/PDGF treatment. Repeated measures ANOVA. n=3. (C): SMILR expression following p38 inhibition. Repeated measures ANOVA. ***P<0.01 vs 0.2% media, ### P<0.001 vs IL1/PDGF treatment alone n=3. (D): SMILR expression in conditioned media from HSVSMC cultured in 0.2%, IL1 or PDGF conditions. Unpaired t test * P<0.05 vs. 0.2% (n=4). (E): Confirmation of the effect of siRNA targeting SMILR in HSVSMC using qRT-PCR (*n=3*). One way ANOVA ***P <0.001 vs. 0.2% control. ### P<0.001 vs IL1 + PDGF treatment. (F): IL1/PDGF induced proliferation classed as 100% for analysis across patient samples, knockdown of *SMILR* inhibits EdU incorporation in HSVSMC (*n=3*) One way ANOVA vs Si Control. ## P<0.01 (G): qRT-PCR analysis of SMILR expression following infection with either an empty lentivirus (LV-E) or lentivirus containing SMILR sequence (LV-S) at

an MOI of 25 (n=3) and MOI 50 (n=3) ***P<0.001 vs. relevant empty control assessed via multiple comparison ANOVA.

Figure 6. *SMILR* regulates proximal gene *HAS2* in chromosome 8. (A): Schematic view of the 8q24.1 region showing lncRNAs and protein coding genes over the 5,000,000 bp region from Ensemble. (B): Regulation of protein coding and non-coding genes within the selected region following IL1α and PDGF treatment, heatmap depicts expression of genes found with RNA-seq in 4 patient samples. (C): Dotted line marks region containing *SMILR* lincRNA and closest protein coding genes *HAS2* and *ZHX2*. (D): Expression of proximal gene *HAS2* - modulated in the same manner as *SMILR* with IL1α and PDGF treatment (n=3). Un-paired t-test ***P<0.001 vs. 0.2% (E-F): Additional HAS isoforms are differentially modulated by IL1 and PDGF (n=3). Unpaired t test ***P<0.001 vs. 0.2% (G-I): Validation of RNA seq data for lncRNAs SMILR and HAS2-AS1 by qRT-PCR (n=3). *<0.05 and ** P<0.01 vs 0.2%,Un-paired t test. (J): Inhibition of SMILR expression via dsiRNA treatment significantly inhibits HAS2 expression determined by qRT-PCR **P<0.01 vs. Si Control. Un-paired t test (n=3). (K-N): SMILR inhibition had no effect on proximal genes ZHX2 or HAS2-AS1 nor additional HAS isoforms, HAS1 or HAS3 (n=3). Un-paired t test.

Figure 7. Uptake [18F]-Fluoride and [18F]-FDG within plaque and normal artery and changes in non-coding RNA expression within carotid plaques. Axial images demonstrating unilateral (A, B) or bilateral [18F]-Fluoride carotid uptake (D, E). Image C is a multi-planar reformat of B. Axial images demonstrating [18F]-FDG carotid uptake (F, G). H shows the Siemens Biograph Clinical PET/CT system used for imaging. White arrows indicate carotid radio-ligand uptake.

(H-K): Uptake of tracer (L): MicroRNA profile of atherosclerotic plaque and paired healthy carotid controls (*n=6*) assessed by qRT-PCR (paired students t test). Expression of *SMILR* (M), *HAS2* (N) and *HAS2-AS1*(O) within atherosclerotic plaque (*n=5*). analysed via qRT-PCR analysis, *** P<0.001, ** P<0.01 and * P<0.05 assessed by paired students t test.

Figure 8. SMILR is detectable within plasma samples and correlates with patient CRP levels. (A): SMILR expression is increased in patients with higher CRP levels (n=13 CRP<2, n=13 CRP2-5 and n=15 CRP>5, *P<0.05, **P<0.01 via One-way ANOVA). (B): Correlation between SMILR expression and CRP levels (linear regression P<0.0001).

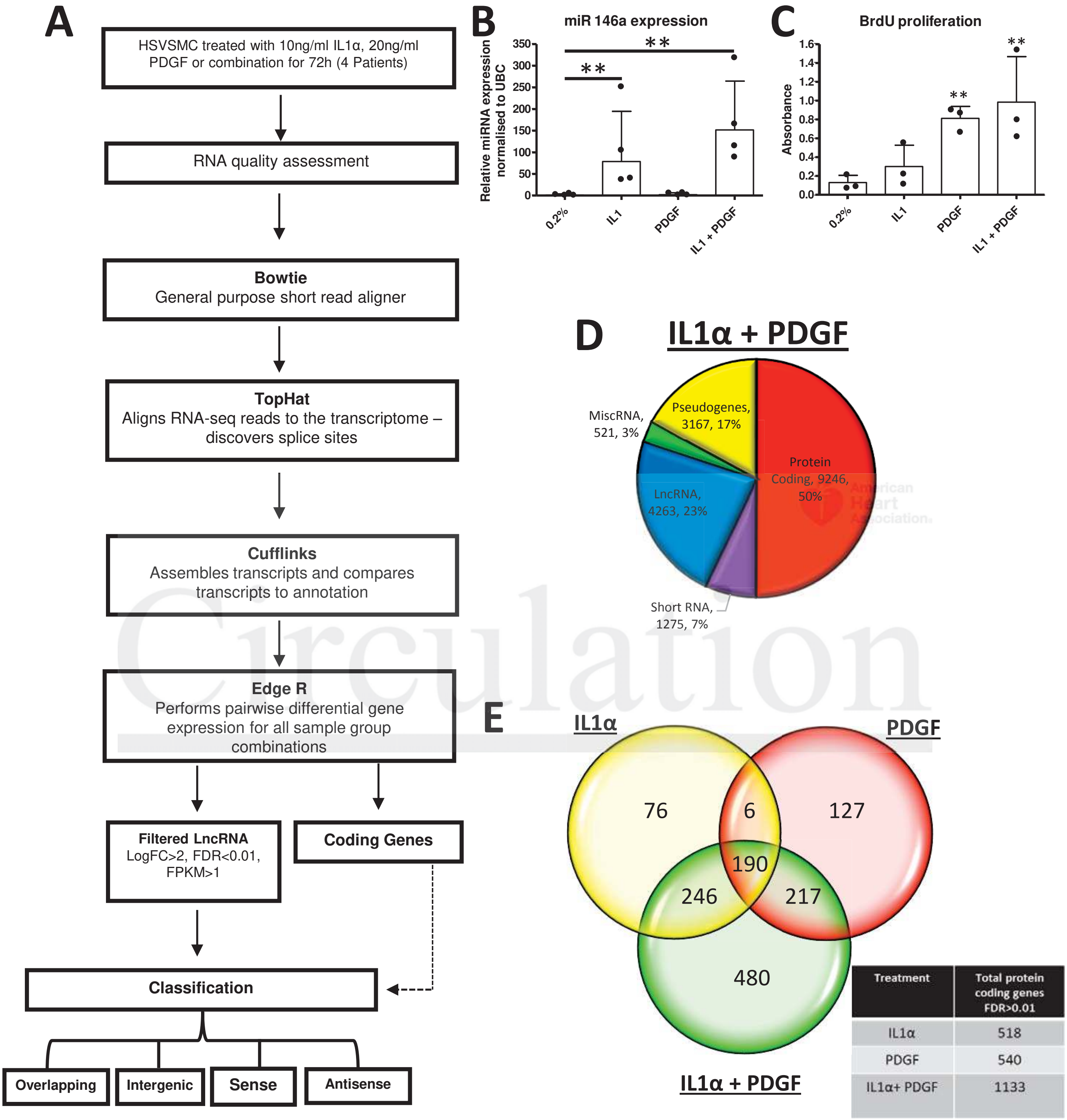

Treatment	Total protein coding genes FDR>0.01
IL1α	518
PDGF	540
IL1α+ PDGF	1133

Figure 1

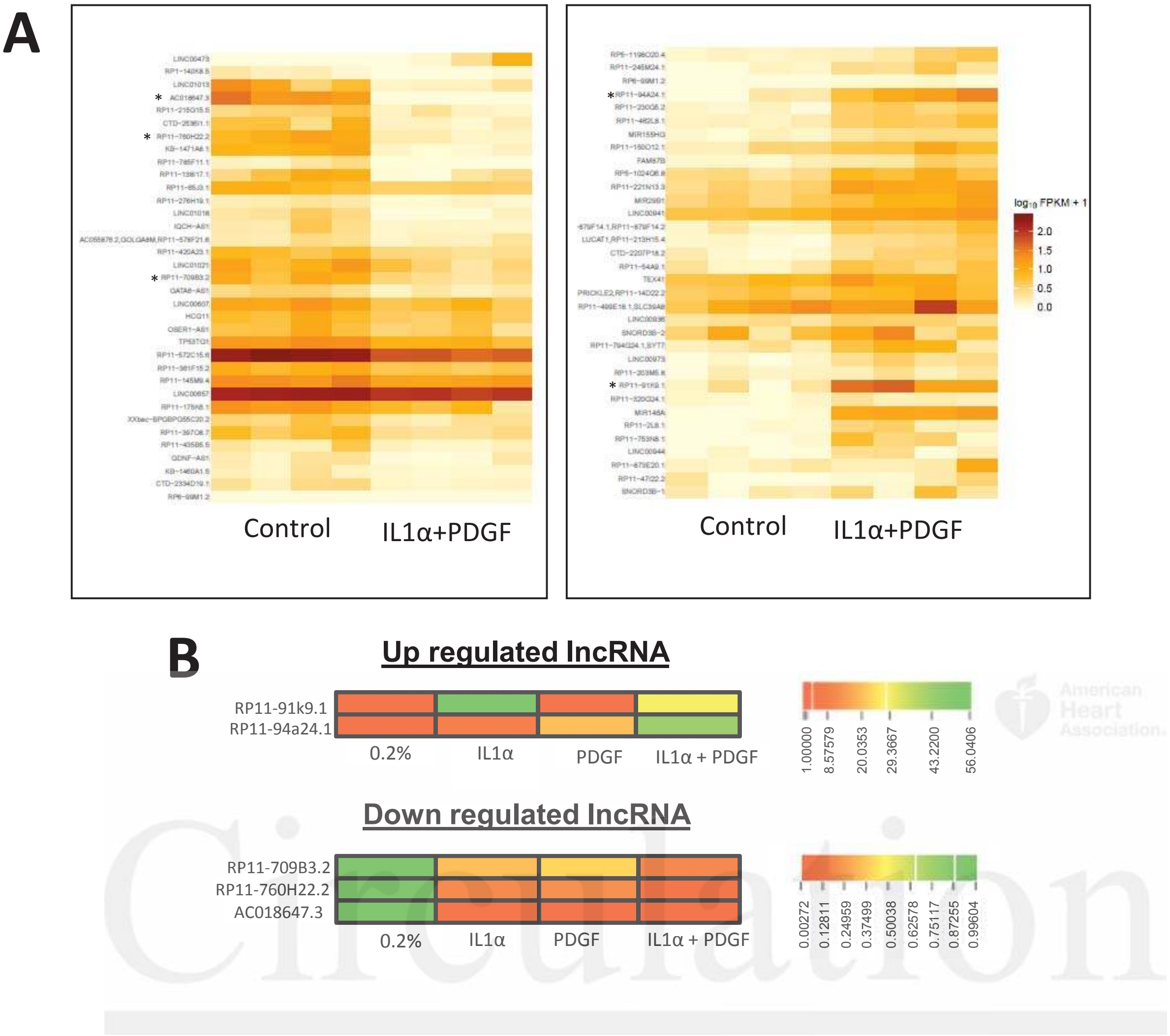A
LINC00473
RP1-140K8.5
LINC01013
* AC018647.3
RP11-215G15.5
CTD-2536I1.1
* RP11-760H22.2
KB-1471A8.1
RP11-785F11.1
RP11-138I17.1
RP11-65J3.1
RP11-276H19.1
LINC01018
IQCH-AS1
AC055876.2,GOLGA8M,RP11-578F21.6
RP11-420A23.1
LINC01021
* RP11-709B3.2
GATA6-AS1
LINC00607
HCG11
OSER1-AS1
TP53TG1
RP11-572C15.6
RP11-381F15.2
RP11-145M9.4
LINC00657
RP11-175K6.1
XXbac-BPGBPG55C20.2
RP11-397O8.7
RP11-435B5.5
GDNF-AS1
KB-1460A1.5
CTD-2334D19.1
RP6-99M1.2
Control
IL1α+PDGF
RP5-1198O20.4
RP11-245M24.1
RP6-99M1.2
* RP11-94A24.1
RP11-230G5.2
RP11-482L8.1
MIR155HG
RP11-150O12.1
FAM87B
RP5-1024G6.8
RP11-221N13.3
MIR29B1
LINC00941
-679F14.1,RP11-679F14.2
LUCAT1,RP11-213H15.4
CTD-2207P18.2
RP11-54A9.1
TEX41
PRICKLE2,RP11-14D22.2
RP11-499E18.1,SLC39A8
LINC00938
SNORD3B-2
RP11-794G24.1,SYT7
LINC00973
RP11-303M5.8
* RP11-91K9.1
RP11-320G24.1
MIR146A
RP11-2L8.1
RP11-753N8.1
LINC00944
RP11-673E20.1
RP11-47I22.2
SNORD3B-1
Control
IL1α+PDGF
$\log_{10}$ FPKM + 1
2.0
1.5
1.0
0.5
0.0
B
Up regulated lncRNA
RP11-91k9.1
RP11-94a24.1
0.2%
IL1α
PDGF
IL1α + PDGF
1.00000
8.57579
20.0353
29.3667
43.2200
56.0406
Down regulated lncRNA
RP11-709B3.2
RP11-760H22.2
AC018647.3
0.2%
IL1α
PDGF
IL1α + PDGF
0.00272
0.12811
0.24959
0.37499
0.50038
0.62578
0.75117
0.87255
0.99604

Figure 2

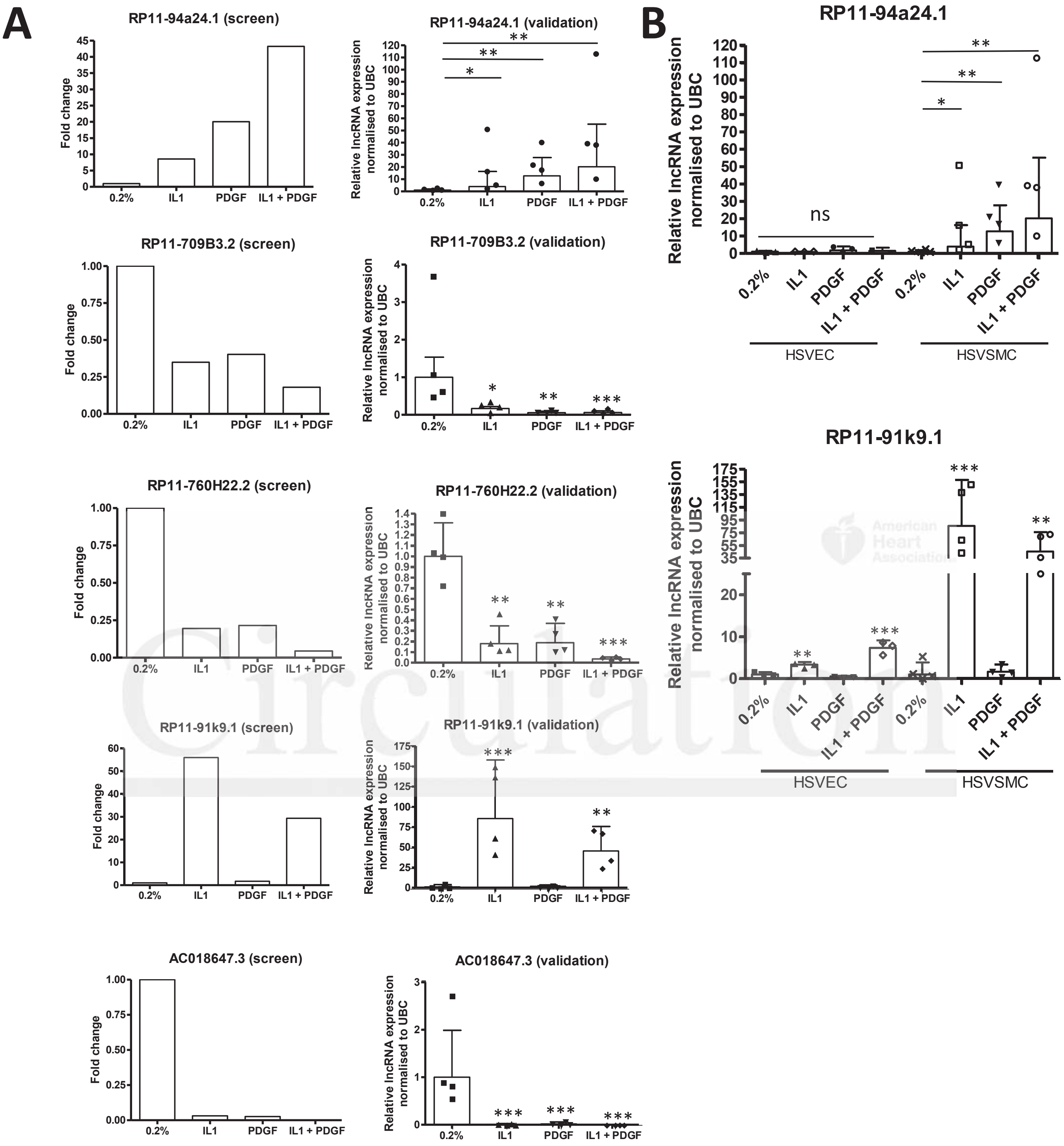
A
RP11-94a24.1 (screen)
Fold change
0
5
10
15
20
25
30
35
40
45
0.2%
IL1
PDGF
IL1 + PDGF
RP11-94a24.1 (validation)
Relative lncRNA expression normalised to UBC
0
10
20
30
40
50
60
70
80
90
100
110
120
*
**
**
0.2%
IL1
PDGF
IL1 + PDGF
RP11-709B3.2 (screen)
Fold change
0.00
0.25
0.50
0.75
1.00
0.2%
IL1
PDGF
IL1 + PDGF
RP11-709B3.2 (validation)
Relative lncRNA expression normalised to UBC
0
1
2
3
4
*
**
***
0.2%
IL1
PDGF
IL1 + PDGF
RP11-760H22.2 (screen)
Fold change
0.00
0.25
0.50
0.75
1.00
0.2%
IL1
PDGF
IL1 + PDGF
RP11-760H22.2 (validation)
Relative lncRNA expression normalised to UBC
0.0
0.1
0.2
0.3
0.4
0.5
0.6
0.7
0.8
0.9
1.0
1.1
1.2
1.3
1.4
**
**
***
0.2%
IL1
PDGF
IL1 + PDGF
RP11-91k9.1 (screen)
Fold change
0
10
20
30
40
50
60
0.2%
IL1
PDGF
IL1 + PDGF
RP11-91k9.1 (validation)
Relative lncRNA expression normalised to UBC
0
25
50
75
100
125
150
175
***
**
0.2%
IL1
PDGF
IL1 + PDGF
AC018647.3 (screen)
Fold change
0.00
0.25
0.50
0.75
1.00
0.2%
IL1
PDGF
IL1 + PDGF
AC018647.3 (validation)
Relative lncRNA expression normalised to UBC
0
1
2
3
***
***
***
0.2%
IL1
PDGF
IL1 + PDGF
B
RP11-94a24.1
Relative lncRNA expression normalised to UBC
0
10
20
30
40
50
60
70
80
90
100
110
120
ns
*
**
**
0.2%
IL1
PDGF
IL1 + PDGF
0.2%
IL1
PDGF
IL1 + PDGF
HSVEC
HSVSMC
RP11-91k9.1
Relative lncRNA expression normalised to UBC
0
10
20
35
55
75
95
115
135
155
175
**
***
***
**
0.2%
IL1
PDGF
IL1 + PDGF
0.2%
IL1
PDGF
IL1 + PDGF
HSVEC
HSVSMC

Figure 3

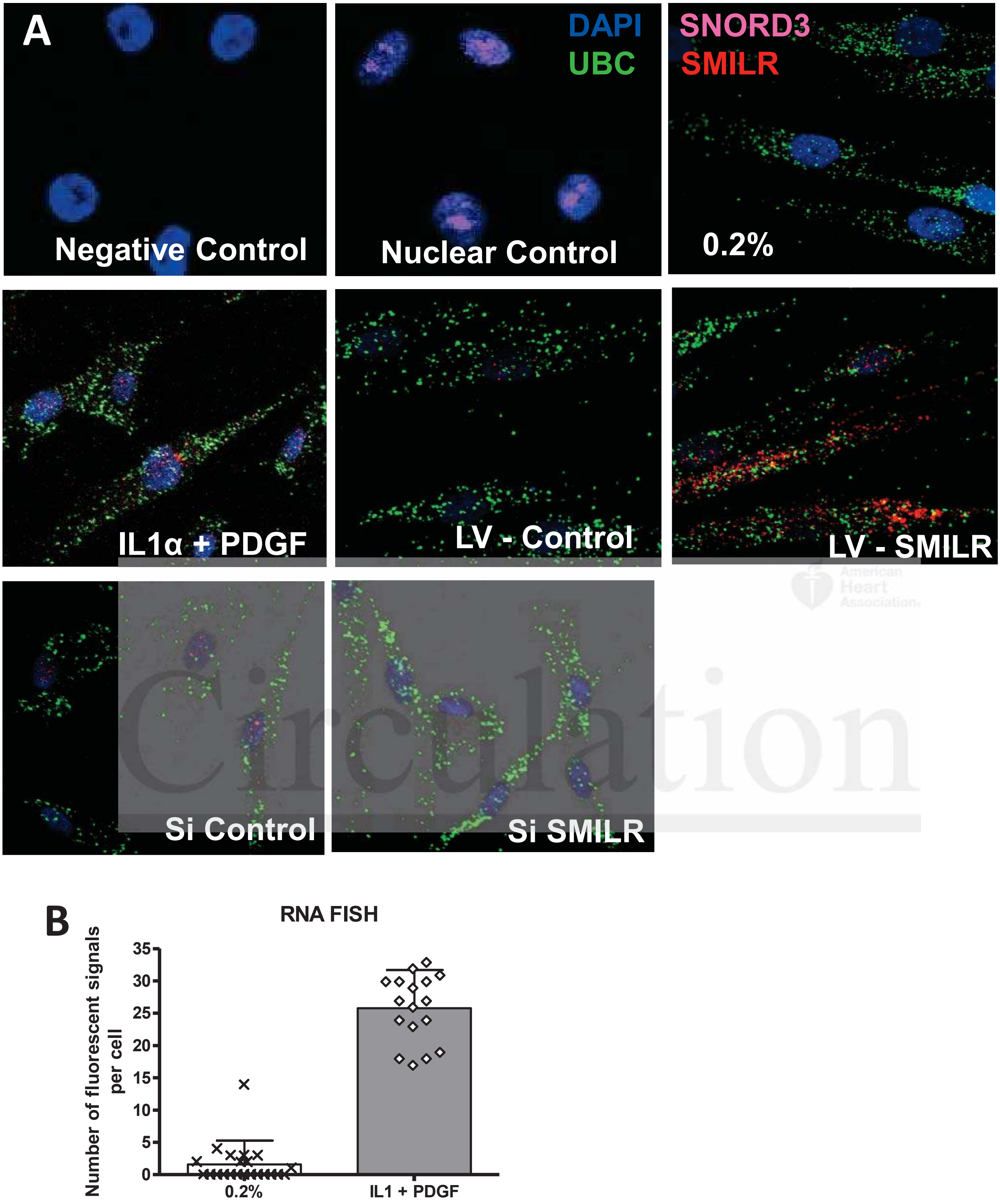
A
Negative Control
DAPI
UBC
Nuclear Control
SNORD3
SMILR
0.2%
IL1α + PDGF
LV - Control
LV - SMILR
Si Control
Si SMILR
B
RNA FISH
Number of fluorescent signals per cell
35
30
25
20
15
10
5
0
0.2%
IL1 + PDGF

Figure 4

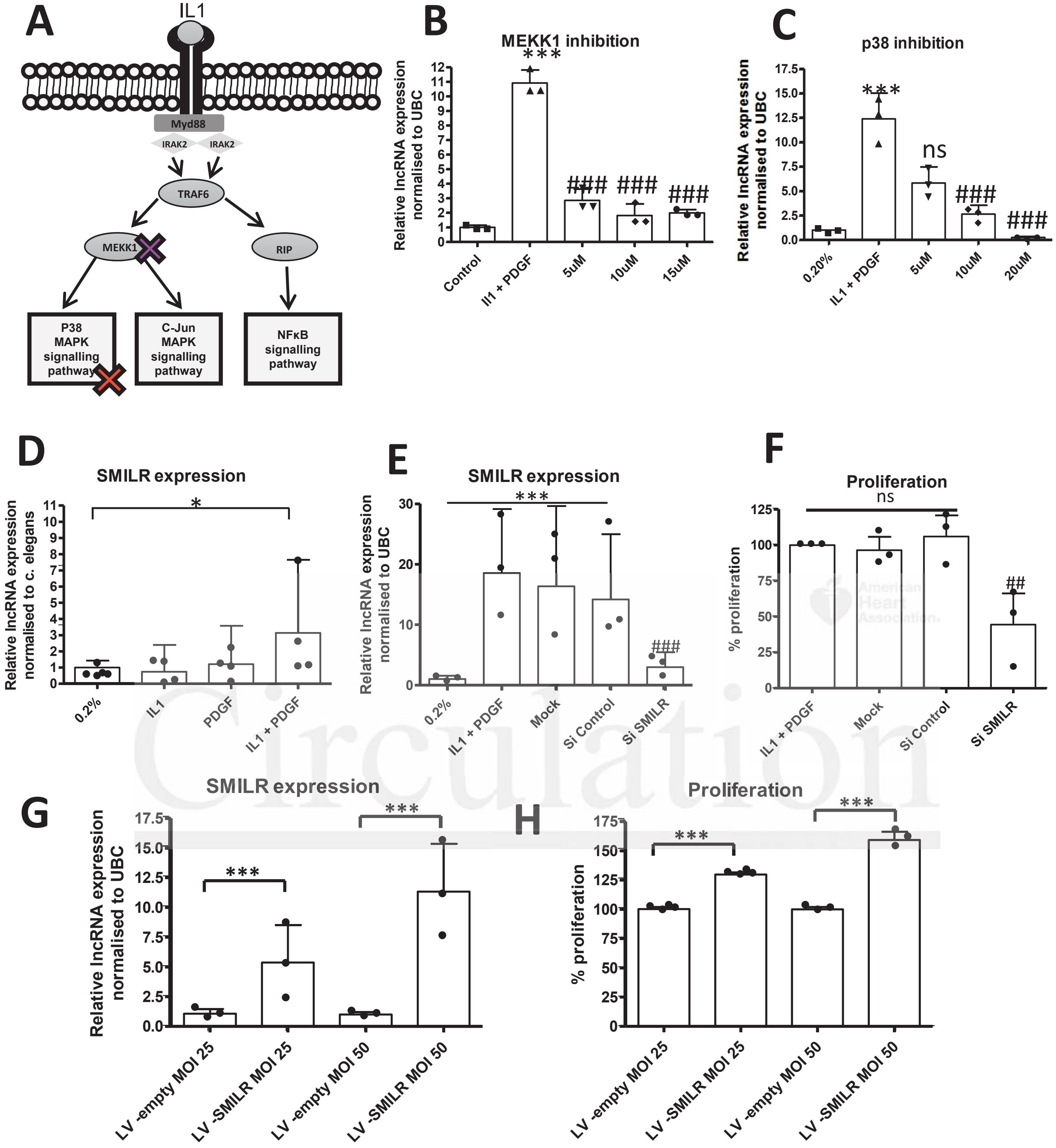
A
IL1
Myd88
IRAK2
IRAK2
TRAF6
MEKK1
RIP
P38 MAPK signalling pathway
C-Jun MAPK signalling pathway
NFκB signalling pathway
B
MEKK1 inhibition
Relative lncRNA expression normalised to UBC
0 1 2 3 4 5 6 7 8 9 10 11 12
***
###
###
###
Control
Il1 + PDGF
5uM
10uM
15uM
C
p38 inhibition
Relative lncRNA expression normalised to UBC
0.0 2.5 5.0 7.5 10.0 12.5 15.0 17.5
***
ns
###
###
0.20%
IL1 + PDGF
5uM
10uM
20uM
D
SMILR expression
Relative lncRNA expression normalised to c. elegans
0 1 2 3 4 5 6 7 8 9 10 11
*
0.2%
IL1
PDGF
IL1 + PDGF
E
SMILR expression
Relative lncRNA expression normalised to UBC
0 10 20 30
***
###
0.2%
IL1 + PDGF
Mock
Si Control
Si SMILR
F
Proliferation
ns
% proliferation
0 25 50 75 100 125
##
IL1 + PDGF
Mock
Si Control
Si SMILR
G
SMILR expression
Relative lncRNA expression normalised to UBC
0.0 2.5 5.0 7.5 10.0 12.5 15.0 17.5
***
***
LV -empty MOI 25
LV -SMILR MOI 25
LV -empty MOI 50
LV -SMILR MOI 50
H
Proliferation
% proliferation
0 25 50 75 100 125 150 175
***
***
LV -empty MOI 25
LV -SMILR MOI 25
LV -empty MOI 50
LV -SMILR MOI 50

Figure 5

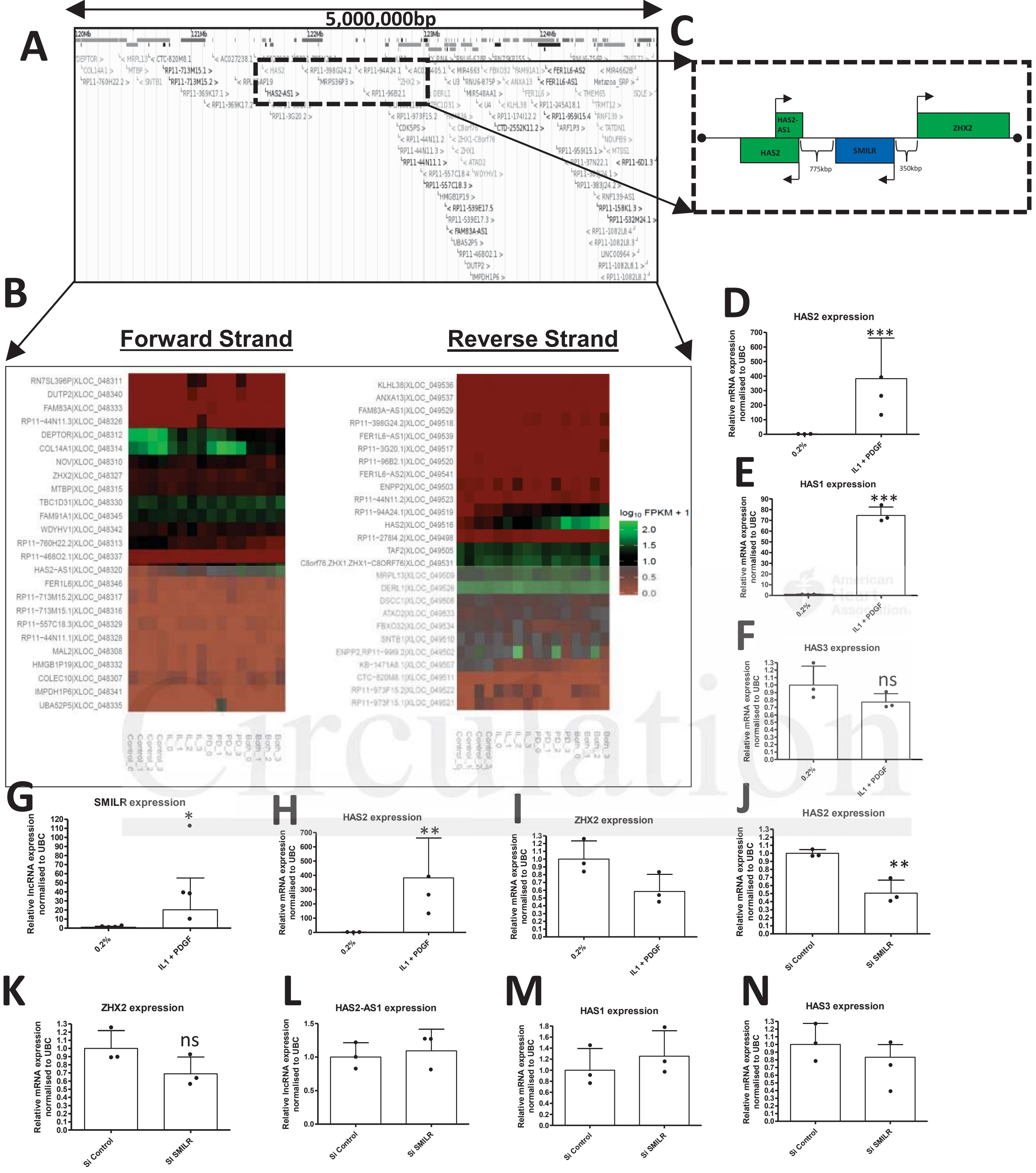5,000,000bp
A
120Mb
121Mb
122Mb
123Mb
124Mb
HAS2
HAS2-AS1
ZHX2
C
HAS2-AS1
HAS2
SMILR
ZHX2
775kbp
350kbp
B
Forward Strand
Reverse Strand
RN7SL396P|XLOC_048311
DUTP2|XLOC_048340
FAM83A|XLOC_048333
RP11-44N11.3|XLOC_048326
DEPTOR|XLOC_048312
COL14A1|XLOC_048314
NOV|XLOC_048310
ZHX2|XLOC_048327
MTBP|XLOC_048315
TBC1D31|XLOC_048330
FAM91A1|XLOC_048345
WDYHV1|XLOC_048342
RP11-760H22.2|XLOC_048313
RP11-468O2.1|XLOC_048337
HAS2-AS1|XLOC_048320
FER1L6|XLOC_048346
RP11-713M15.2|XLOC_048317
RP11-713M15.1|XLOC_048316
RP11-557C18.3|XLOC_048329
RP11-44N11.1|XLOC_048328
MAL2|XLOC_048308
HMGB1P19|XLOC_048332
COLEC10|XLOC_048307
IMPDH1P6|XLOC_048341
UBA52P5|XLOC_048335
KLHL38|XLOC_049536
ANXA13|XLOC_049537
FAM83A-AS1|XLOC_049529
RP11-398G24.2|XLOC_049518
FER1L6-AS1|XLOC_049539
RP11-3G20.1|XLOC_049517
RP11-96B2.1|XLOC_049520
FER1L6-AS2|XLOC_049541
ENPP2|XLOC_049503
RP11-44N11.2|XLOC_049523
RP11-94A24.1|XLOC_049519
HAS2|XLOC_049516
RP11-278I4.2|XLOC_049498
TAF2|XLOC_049505
C8orf76.ZHX1.ZHX1-C8ORF76|XLOC_049531
MRPL13|XLOC_049509
DERL1|XLOC_049526
DSCC1|XLOC_049506
ATAD2|XLOC_049533
FBXO32|XLOC_049534
SNTB1|XLOC_049510
ENPP2,RP11-999.2|XLOC_049502
KB-1471A8.1|XLOC_049507
CTC-820M8.1|XLOC_049511
RP11-973F15.2|XLOC_049522
RP11-973F15.1|XLOC_049521
Control_0
Control_1
Control_2
Control_3
IL_0
IL_1
IL_2
IL_3
PD_0
PD_1
PD_2
PD_3
Both_0
Both_1
Both_2
Both_3
log10 FPKM + 1
2.0
1.5
1.0
0.5
0.0
D
HAS2 expression
***
E
HAS1 expression
***
F
HAS3 expression
ns
G
SMILR expression
*
H
HAS2 expression
**
I
ZHX2 expression
J
HAS2 expression
**
K
ZHX2 expression
ns
L
HAS2-AS1 expression
M
HAS1 expression
N
HAS3 expression
Relative mRNA expression normalised to UBC
Relative lncRNA expression normalised to UBC
0.2%
IL1 + PDGF
Si Control
Si SMILR

Figure 6

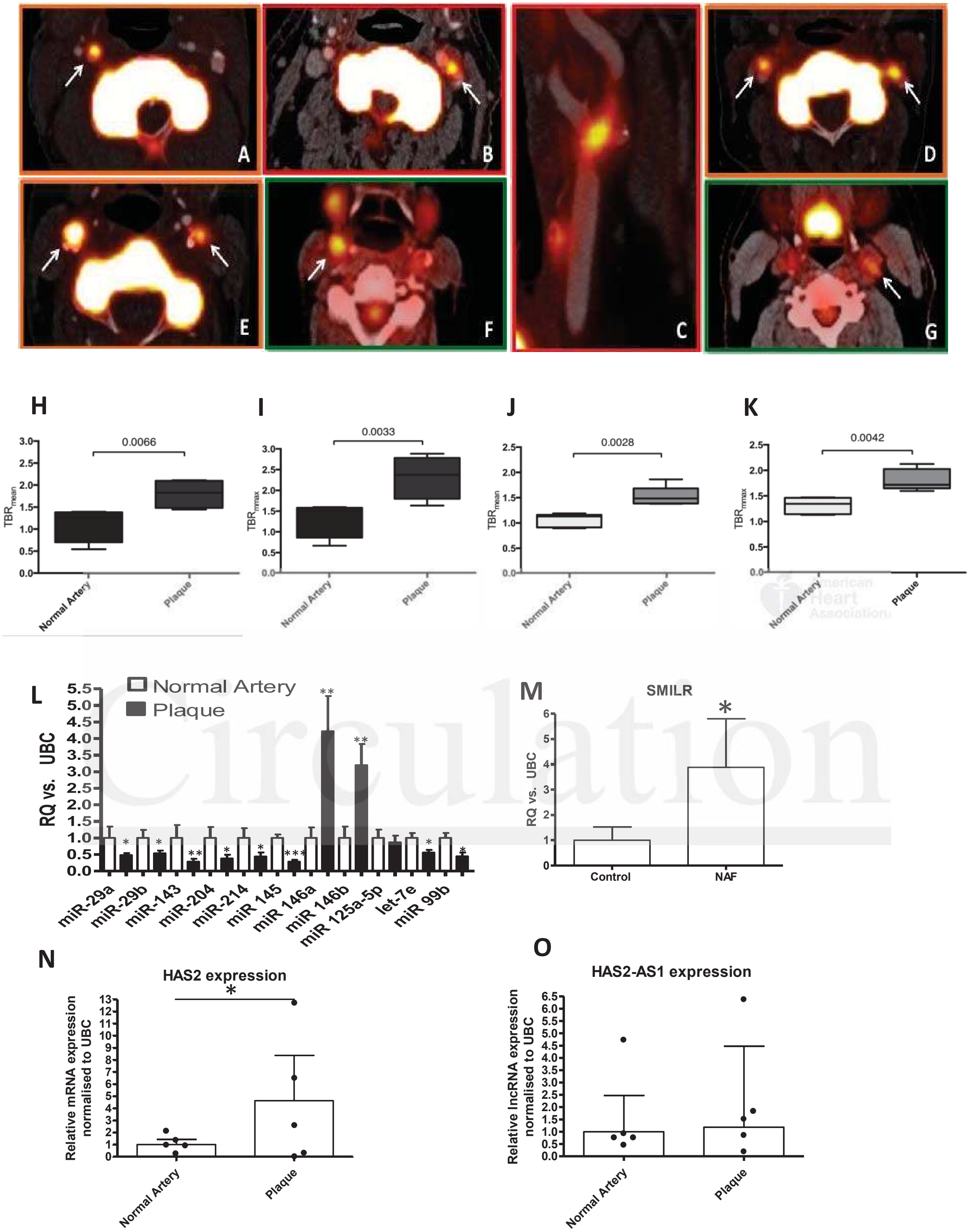
A
B
C
D
E
F
G
H
0.0066
TBR$_{mean}$
3.0
2.5
2.0
1.5
1.0
0.5
0.0
Normal Artery
Plaque
I
0.0033
TBR$_{mmax}$
Normal Artery
Plaque
J
0.0028
TBR$_{mean}$
Normal Artery
Plaque
K
0.0042
TBR$_{mmax}$
Normal Artery
Plaque
L
Normal Artery
Plaque
RQ vs. UBC
5.5
5.0
4.5
4.0
3.5
3.0
2.5
2.0
1.5
1.0
0.5
0.0
*
**
***
miR-29a
miR-29b
miR-143
miR-204
miR-214
miR 145
miR 146a
miR 146b
miR 125a-5p
let-7e
miR 99b
M
SMILR
RQ vs. UBC
Control
NAF
N
HAS2 expression
Relative mRNA expression normalised to UBC
Normal Artery
Plaque
O
HAS2-AS1 expression
Relative lncRNA expression normalised to UBC
Normal Artery
Plaque

Figure 7

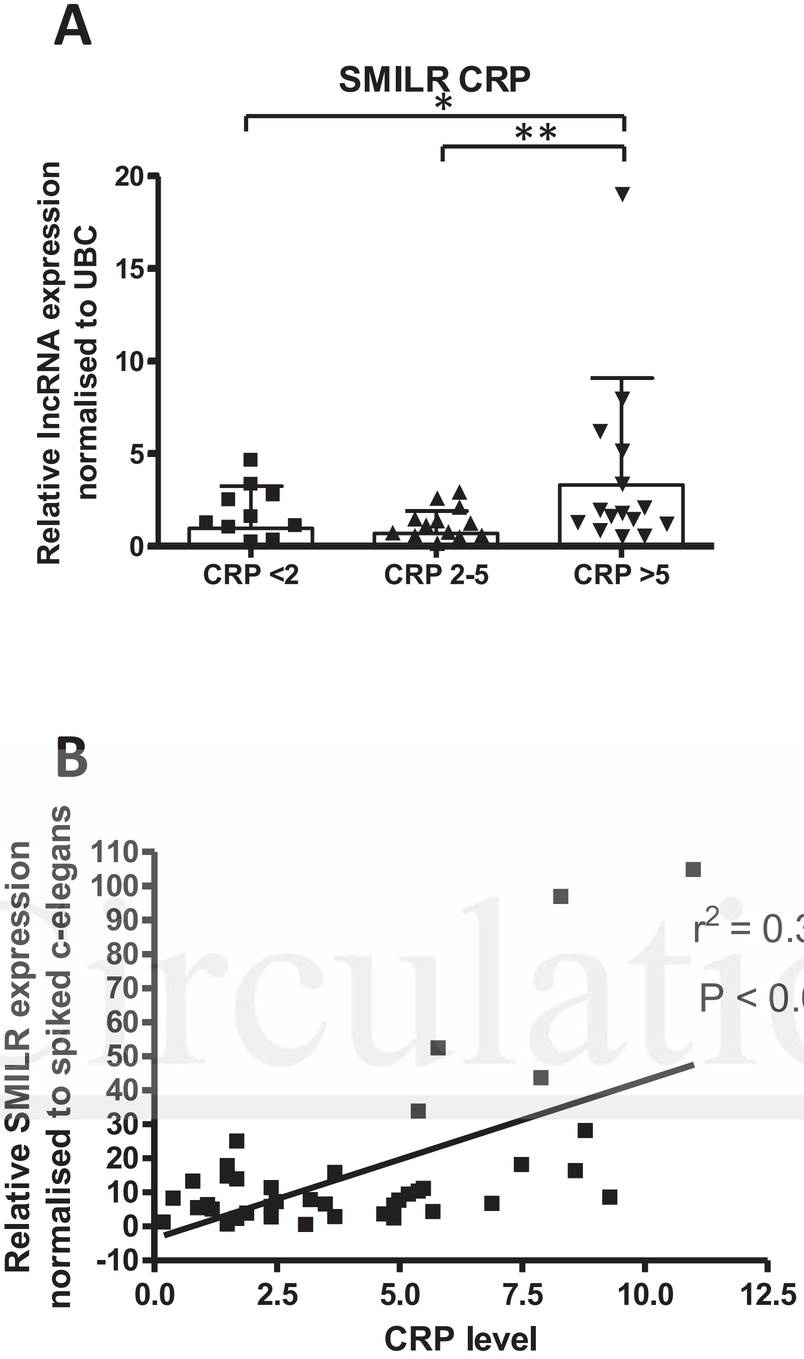
A
SMILR CRP
*
**
Relative lncRNA expression normalised to UBC
20
15
10
5
0
CRP <2
CRP 2-5
CRP >5
B
Relative SMILR expression normalised to spiked c-elegans
110
100
90
80
70
60
50
40
30
20
10
0
-10
0.0
2.5
5.0
7.5
10.0
12.5
CRP level
r2 = 0.3270
P < 0.0001

Figure 8

Circulation
JOURNAL OF THE AMERICAN HEART ASSOCIATION

American Heart Association®

Smooth Muscle Enriched Long Non-Coding RNA (*SMILR*) Regulates Cell Proliferation

Margaret D. Ballantyne, Karine Pinel, Rachel Dakin, Alex T. Vesey, Louise Diver, Ruth Mackenzie, Raquel Garcia, Paul Welsh, Naveed Sattar, Graham Hamilton, Nikhil Joshi, Marc R. Dweck, Joseph M. Miano, Martin W. McBride, David E. Newby, Robert A. McDonald and Andrew H. Baker

Circulation. published online April 6, 2016;
Circulation is published by the American Heart Association, 7272 Greenville Avenue, Dallas, TX 75231

Print ISSN: 0009-7322. Online ISSN: 1524-4539

SUPPLEMENTAL MATERIAL

Supplemental Methods

Tissue and Cell culture

Endothelial media supplemented 20% FCS (Life Technologies, Paisley, UK). HSVSMC media supplemented with 15% foetal bovine serum (FBS) (PAA laboratories, Yeovil, UK), 2 mM L-Glutamine (Invitrogen, Paisley, UK) 50 µg/ml penicillin (Invitrogen) and 50 µg/mL streptomycin (Invitrogen). All cells were used between passages 3-5.

HSVSMC BrdU and EdU Incorporation assay

HSVSMC proliferation was quantified using a DNA bromodeoxyuride (BrdU) incorporation assay (Millipore, Watford, UK), or EdU according to the manufacturer's instructions. Briefly, cells were plated and quiesced in 0.2% FCS media for 48 h prior to stimulation. Cells were stimulated with either 10 ng/mL IL1α, 20 ng/mL PDGF or a combination of both for the stated times. For BrdU experiments, 6 h after stimulation cells were incubated with BrdU and for EdU experiments EdU was added at the point of stimulation for the remaining time to allow cell proliferation. BrdU: after removing the culture medium, the cells were fixed followed by incubation with anti-BrdU antibody which binds the incorporated DNA. After adding the substrate solution, the immune complexes were detected using a plate reader set at dual wavelength of 450/550 nm, Victor (Perkin Elmer, Waltham, USA). EdU: following stimulation, cellular RNA was extracted as described earlier or fixed in 70% ethanol for EdU FACs analysis. EdU incorporation was quantified using Click-it EdU Proliferation assay with an Alexa Fluor 594 antibody according to the manufacturer's protocol (Life Technologies).

MEKK1 and P38 inhibitor studies

For inhibitor studies, HSVSMC were plated and quiesced for 48 h. One hour prior to stimulation, cells were incubated with either 10, 15 or 20 µM AZD6244 (MEKK1 inhibitor, Selleckchem, Suffolk, UK) or 5, 10 or 20 µM P38 (SB 203580). Cells were then maintained in either 0.2% media or stimulated with a combination of IL1α and PDGF for 24 h before RNA isolation.

5’ and 3’ RACE

5’ 3’ Rapid amplification of cDNA ends [1] was performed to determine the full length transcript of SMILR using the SMARTer RACE 5’/3’ Kit (Clontech, Saint-Germain-en-Laye, France) according to manufacturer’s instructions. Nested PCR was used to ensure only specific 5’ and 3’ products were detected (*PCR Primer sequence – Suppl. Table 1*). Following cloning into supplied cloning vector, products were sequenced.

Fluorescent *in situ* hybridisation

Custom RNA-FISH tiled probe sets were generated to all exons of SMILR. RNA FISH utilises “branch tree” technology. Briefly, a target specific probe set, containing 40 oligo probes, hybridises to the target mRNA as 20 oligo pairs. Each oligo pair forms a required platform for assembly of the signal amplification structure (tree) through a series of sequential hybridisation steps. Each fully assembled structure, covers a space of 40-50 nt of the target RNA, and has the capacity for 400-fold signal amplification. Therefore, a typical RNA probe set (containing 20 oligo pairs) has the capacity to generate 8,000-fold signal amplification. Due to this technology the company confirms single-molecule RNA sensitivity, thus each fluorescent signal corresponds to an individual lncRNA molecule.

Control SNORD3 and UBC were used as housekeepers to determine spatial location of SMILR (Panomics, Affymetrix, California, US). RNA-FISH was performed according to manufacturer's instructions (ViewRNA^{TM} cell FISH) with minor modifications for both cell and tissue experiments. For cellular analysis, HSVSMC ± IL1α/PDGF were grown on 16-mm coverslips to 80% confluency, washed in PBS and fixed in 4% paraformaldehyde supplemented with 1% glacial acetic acid. Following detergent QS permeabilisation and 1:6000 protease digest, coverslips were incubated with a combination of UBC and SMILR probe sets or UBC. Probe set buffer was used as a negative control and SNORD3 as confirmation of nuclear permeabilisation. Following probe hybridisation, cover slips were incubated with branched tree technology pre amplifier for 1 h and amplifier for 30 min. Cover slips were finally incubated with fluorescent probes, mounted onto glass slides using Prolong gold anti-fade with DAPI mounting medium (Life Technologies).

Image acquisition

Images acquired on a Zeiss 510 confocal system. At least 5 images were taken per condition. Parameters for acquisition and post analysis were identical for all conditions. Images were Z stacked to confirm nuclear localisation.

Dicer substrate siRNA (dsiRNA) mediated transfection

Double stranded dicer substrate siRNA targeting SMILR and Si-control were synthesised (Integrated DNA Technologies, Leuven, Belgium). The Si-control does not target any sequence in the human, mouse, or rat transcriptomes. Transient transfection was performed with Lipofectamine 2000 (Life Technologies). Cells were transfected with either 25 nM Si-SMILR or Si-Control. Six hours post transfection, cells were quiesced for 48 h and stimulated for a further 48 h with 0.2% media containing IL1α/PDGF.

Lentiviral mediated infection

Lentiviral vectors were produced by triple transient transfection of HEK293T cells with a packaging plasmid (pCMVΔ8.74), a plasmid encoding the envelope of vesicular stomatitis virus (VSVg) (pMDG) (Plasmid Factory, Bielefeld, Germany) and pLNT/SFFV-MCS plasmid employing polyethylenimine (PEI; Sigma-Aldrich, St Louis, USA) as previously described. Lentiviral titres were ascertained by TaqMan quantitative real-time PCR (qRT-PCR) using the following primer/probe sequences: forward, 5'-TGTGTGCCCGTCTGTTGTGT-3'; reverse, 5'- GAGTCCTGCGTCGAGAGAGC-3'; probe, 5'-(FAM)-CAGTGGCGCCCGAACAGGGA- (TAMRA)-3. SMILR was cloned into the pLNT/SFFV-MCS (kind gift from Adrian J. Thrasher, London, UK) plasmid using Platinum taq polymerase, according to manufacturer's instructions, to create pLNT/SFFV-MCS-SMILR. A confluent monolayer of smooth muscle cells were plated and infected with a multiplicity of infection of either 25 or 50, neither of which induced any form of toxicity in our cells. Following 24 h infection, media was changed to 0.2% for a further 48 h. Cells were then stimulated and EdU incorporation or SMILR expression investigated as above.

Detection of LncRNA in exosomes secreted from HSVSMC

SMILR expression in conditioned media utilising both ultracentrifugation and exosome isolation kits. RNA extraction of exosome free HSVSMC media was performed using a standard volume (15 mL). The conditioned media was centrifuged at 2000 g at 4°C for 10 min and then at 12000 g for 45 min to remove all cell debris. The supernatant was filtered (0.22 µm) followed by ultracentrifugation at 110 000 g, 4°C for 90 min (Optima L-80 XP ultracentrifuge Beckman coulter) to obtain microvesicles (MV) and exosomes and exosome free media compartments. Additional experiments were performed utilising the Total exosome isolation kit (Life technologies) following the manufacturer's instructions. The presence of microvesicles and exosomes was verified using the Nanosight technology

For exosomes and microvesicles, 700 µL of Qiazol (Qiagen) was added and 3 µL of c.elegans total RNA at 25 ng/µL and the RNA was extracted using miRNEasy mini kit (Qiagen) as previously described. For the exosome free media compartment, RNA was extracted from 2 mL and following the same protocol as describe in the manuscript. SMILR relative expression was determined in theses 2 compartments by qRT-PCR.

In Vivo Studies Atherosclerosis Studies: Patients, Imaging and Sampling

Carotid cohort

Patients with symptomatic carotid artery stenosis (≥50% by NASCET criteria [2]) scheduled to undergo carotid endarterectomy were recruited from neurovascular clinics at the Royal Infirmary of Edinburgh between January 2013 and April 2014. Exclusion criteria included a modified Rankin score of 3, insulin-dependent diabetes mellitus, women of child-bearing age not receiving contraception, severe chronic kidney disease (eGFR <30 mL/min/1.73 m^2), known iodine-based contrast media allergy, prior ipsilateral carotid intervention, prior neck irradiation, and inability to provide informed consent. Patients underwent a standard baseline clinical assessment including blood sampling (for standard clinical haematological and biochemical indices, including C reactive protein, and plasma RNA analysis) before undergoing separate [18F]-fluoride and [18F]-fluorodeoxyglucose ([18F]-FDG) positron emission tomography [3] combined with computed tomography (CT) scans with the use of a hybrid scanner (Biograph mCT, Siemens Medical Systems, Erlangen, Germany). Both of these tracers have been used by our group and others for plaque imaging and highlight high-risk actively calcifying [4] and inflamed or hypoxic atherosclerotic plaques.

For [18F]-fluoride imaging, a target dose of 250 MBq was administered intravenously. Scanning took place after a 60-min delay. Following an attenuation-correction CT scan (non-enhanced, low dose 120 kV, 50 mAs) PET imaging was performed in static mode covering 2 bed positions (15 min each) with the superior bed centered over the carotid bifurcation.

Following PET acquisition, a CT carotid angiogram was performed without moving the patient (Care Dose 4D, 120 kV, 145 mA, rotation time 0.5 s, pitch 0.8).

[18F]-FDG PET/CT was performed on a separate day. A target dose of 125 MBq was administered intravenously and scanning commenced after a 90-min delay. PET/CT acquisition was identical to [18F]-Fluoride save for a longer bed time of 20-min and a pre-scan fast of 6 h. Static images were reconstructed using the Siemens Ultra-HD algorithm (time of flight + True X) with corrections applied for attenuation, dead time, scatter, and random coincidences.

PET tracer uptake was quantified using an OsiriX workstation (OsiriX version 3.5.1 64-bit; OsiriX Imaging Software, Geneva, Switzerland). PET/CT image data were reviewed for evidence of tracer uptake, image quality and registration. The CT angiogram was examined to establish plaque presence, location and characteristics. Regions of interest [5] were then drawn on three adjacent 3-mm PET slices to incorporate the internal carotid artery plaque. Three ROI were then drawn around adjacent healthy portions of carotid artery and the lumen of the SVC to derive control values for “normal” arterial uptake and the blood pool respectively. Arterial standardized uptake values (SUV) were recorded and also indexed to blood pool activity thus giving a target-to-background-ratio (TBR).

At the time of surgery, plaques were collected immediately following excision and photographed. Two-millimeter diameter core biopsy specimens for RNA analysis were taken from regions of focally high uptake on PET and from normal tissue at the periphery of the endarterectomy specimen. These, along with the main specimen, were immediately frozen and placed in an -80°C fridge for subsequent batch analysis. Patient characteristic found in Suppl. Table. 5.

Assessment of lncRNA in human plasma

A standard volume of each plasma sample (300 µL) was used to extract RNA. Five volumes of QIAzol lysis reagent (Qiagen) was added per extraction and supplemented with spike-in RNA controls: 3.5 µL of miRNeasy Serum/Plasma Spike-In Control at 1.6 x 108 copies/µL (C. elegans miR-39 miRNA mimic; Qiagen) and 3 µL of c.elegans total RNA at 25 ng/µL. Following 5-min incubation at RT, chloroform was added at equal volumes to the starting sample. Following centrifugation (15 min; 8000 g; 4°C) the clear upper aqueous phase was used to isolate RNA as above.

Supplemental Figures

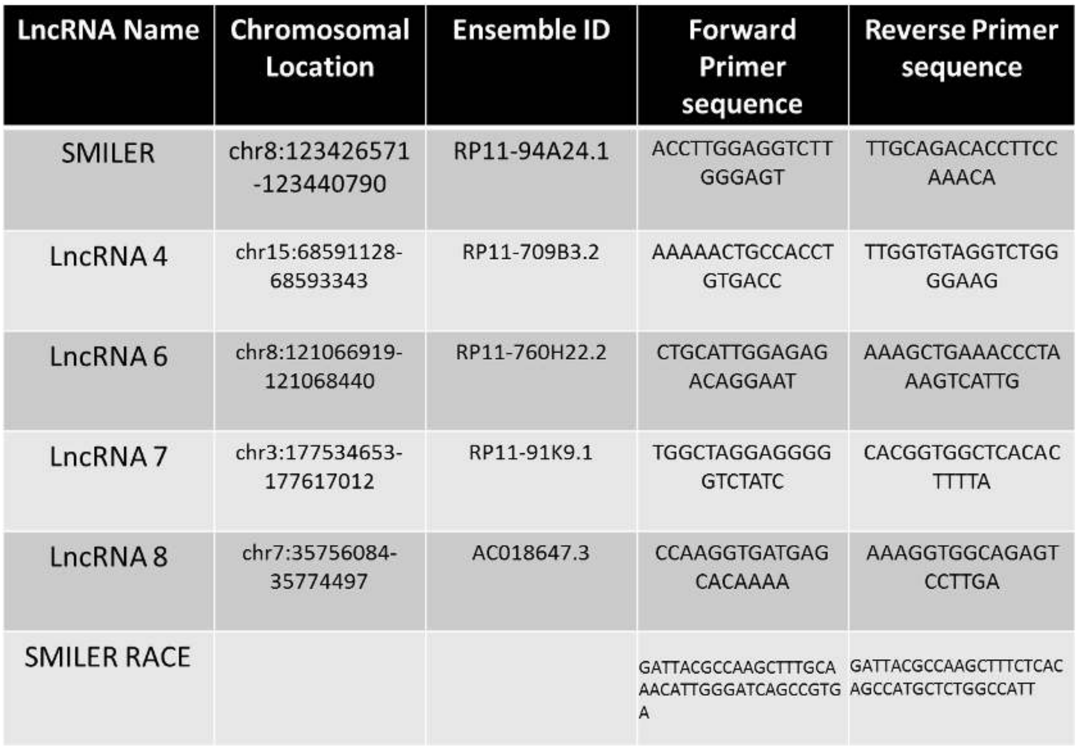

LncRNA Name	Chromosomal Location	Ensemble ID	Forward Primer sequence	Reverse Primer sequence
SMILER	chr8:123426571-123440790	RP11-94A24.1	ACCTTGGAGGTCTTGGGAGT	TTGCAGACACCTTCCAAACA
LncRNA 4	chr15:68591128-68593343	RP11-709B3.2	AAAAACTGCCACCTGTGACC	TTGGTGTAGGTCTGGGGAAG
LncRNA 6	chr8:121066919-121068440	RP11-760H22.2	CTGCATTGGAGAGACAGGAAT	AAAGCTGAAACCCTAAAGTCATTG
LncRNA 7	chr3:177534653-177617012	RP11-91K9.1	TGGCTAGGAGGGGGTCTATC	CACGGTGGCTCACACTTTTA
LncRNA 8	chr7:35756084-35774497	AC018647.3	CCAAGGTGATGAGCACAAAA	AAAGGTGGCAGAGTCCTTGA
SMILER RACE			GATTACGCCAAGCTTTGCAAACATTGGGATCAGCCGTGA	GATTACGCCAAGCTTTCTCACAGCCATGCTCTGGCCATT

Supplemental Table 1: Sybr green primer sequences. Exon spanning lncRNA primers were designed to each lncRNA to ensure no genomic DNA was assessed during qRT-PCR.

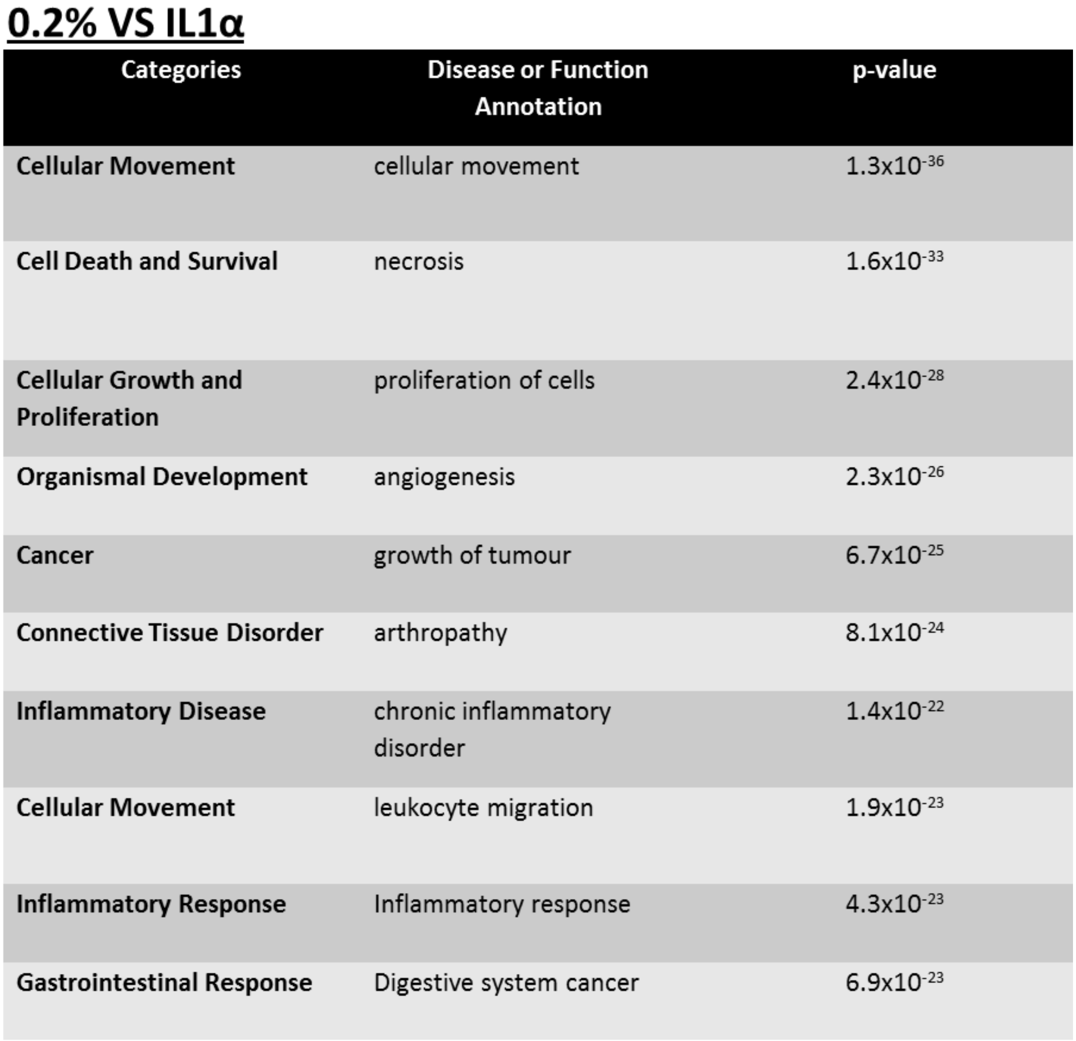

0.2% VS IL1α

Categories	Disease or Function Annotation	p-value
Cellular Movement	cellular movement	1.3x10^{-36}
Cell Death and Survival	necrosis	1.6x10^{-33}
Cellular Growth and Proliferation	proliferation of cells	2.4x10^{-28}
Organismal Development	angiogenesis	2.3x10^{-26}
Cancer	growth of tumour	6.7x10^{-25}
Connective Tissue Disorder	arthropathy	8.1x10^{-24}
Inflammatory Disease	chronic inflammatory disorder	1.4x10^{-22}
Cellular Movement	leukocyte migration	1.9x10^{-23}
Inflammatory Response	Inflammatory response	4.3x10^{-23}
Gastrointestinal Response	Digestive system cancer	6.9x10^{-23}

Supplemental Table 2: IL1α stimulation Ingenuity Pathway analysis. Top 10 disease and functional pathways predicted to be altered by IPA in HSVSM cells stimulated with IL1α.

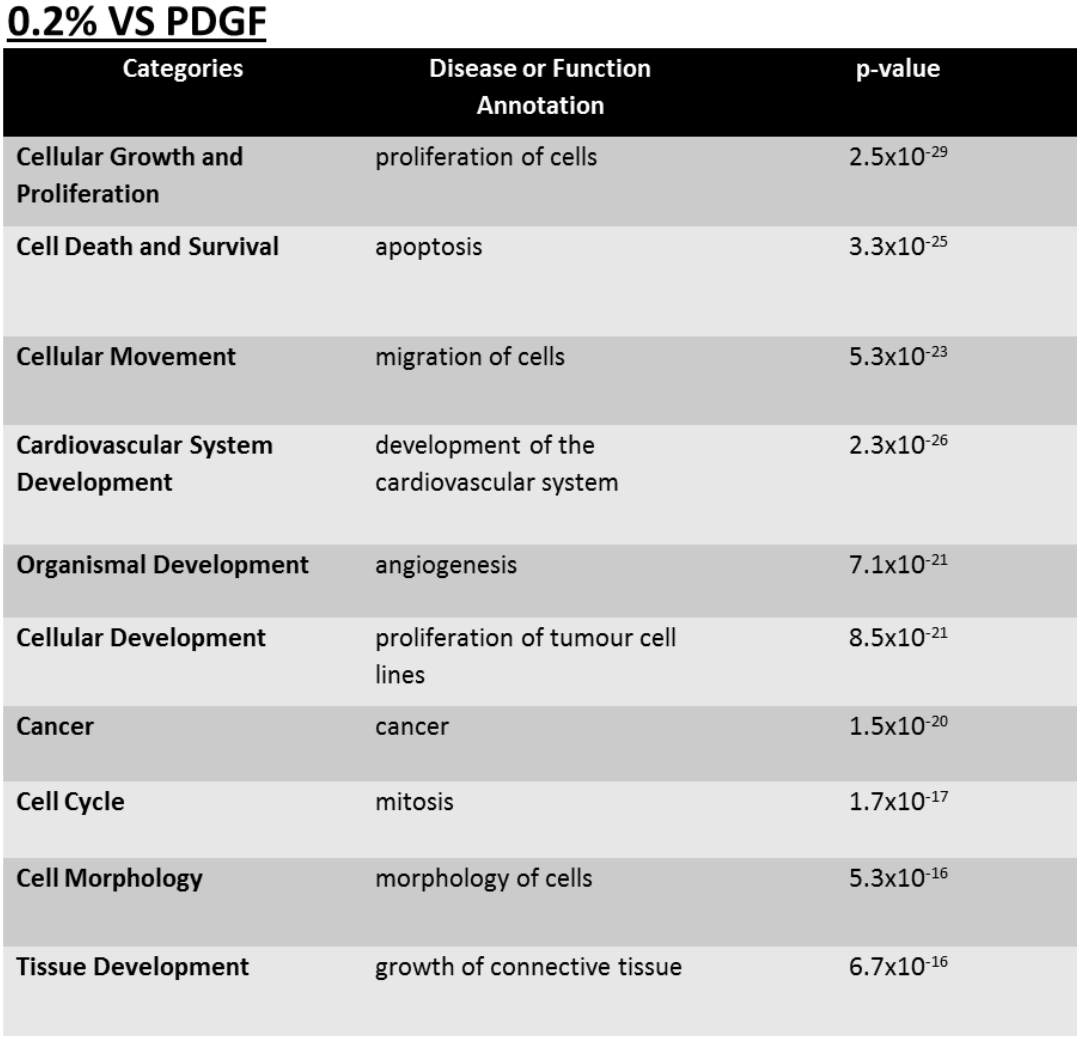

0.2% VS PDGF

Categories	Disease or Function Annotation	p-value
Cellular Growth and Proliferation	proliferation of cells	$2.5\text{x}10^{-29}$
Cell Death and Survival	apoptosis	$3.3\text{x}10^{-25}$
Cellular Movement	migration of cells	$5.3\text{x}10^{-23}$
Cardiovascular System Development	development of the cardiovascular system	$2.3\text{x}10^{-26}$
Organismal Development	angiogenesis	$7.1\text{x}10^{-21}$
Cellular Development	proliferation of tumour cell lines	$8.5\text{x}10^{-21}$
Cancer	cancer	$1.5\text{x}10^{-20}$
Cell Cycle	mitosis	$1.7\text{x}10^{-17}$
Cell Morphology	morphology of cells	$5.3\text{x}10^{-16}$
Tissue Development	growth of connective tissue	$6.7\text{x}10^{-16}$

Supplemental Table 3: PDGF stimulation Ingenuity Pathway analysis. Top 10 disease and functional pathways predicted to be altered by IPA in HSVSM cells stimulated with PDGF.

0.2% VS IL1α + PDGF

Categories	Disease or Function Annotation	p-value
Cellular Growth and Proliferation	proliferation of cells	$1.0x10^{-45}$
Cell Death and Survival	apoptosis	$7.2x10^{-44}$
Cancer	cancer	$1.2x10^{-37}$
Cellular Movement	migration of cells	$2.3x10^{-34}$
Gastrointestinal Response	digestive system cancer	$7.0x10^{-30}$
Cellular Development	proliferation of tumour cell lines	$8.5x10^{-28}$
Reproductive System Disease	tumour	$4.8x10^{-27}$
Cell Cycle	Cell cycle progression	$6.2x10^{-26}$
Cardiovascular System development	morphology of cells	$2.2x10^{-24}$
Cardiovascular System development	angiogenesis	$4.8x10^{-24}$

Supplemental Table 4: IL1α + PDGF stimulation Ingenuity Pathway analysis. Top 10 disease and functional pathways predicted to be altered by IPA in HSVSM cells stimulated with IL1α and PDGF.

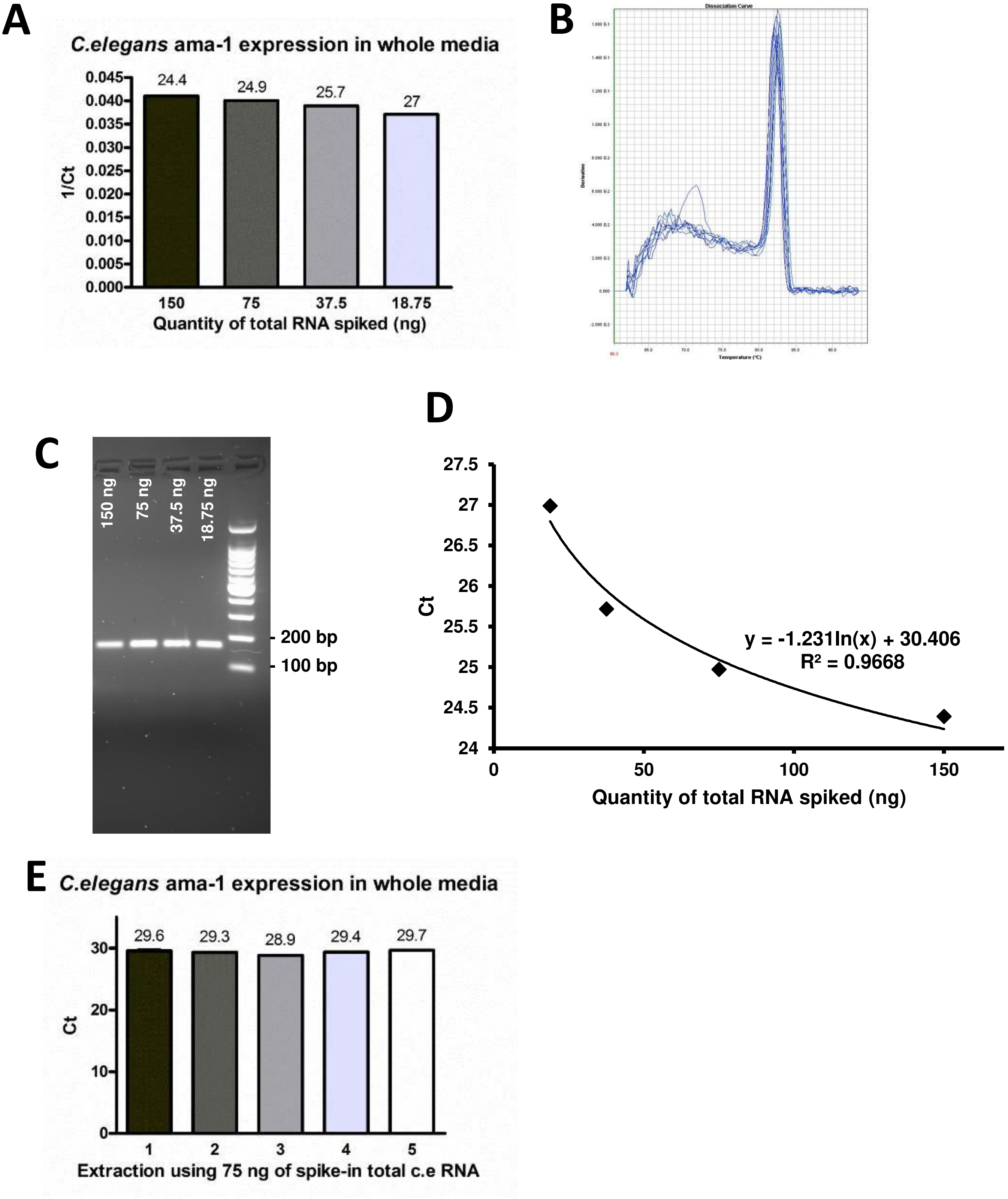

Supplemental Figure 1: Spike-in method of *C.elegans* total RNA in whole HSVSMC media. **(A):** Dose response effect of *C.elegans ama-1* expression. Expression determined by qRT-PCR and results displayed as 1/Ct. Number at the top of each histogram corresponds to Ct values. **(B):** Specificity of products analysis by melting curve. **(C):** Specificity of products analysed using agarose gel. The cDNA amplicon size has been resolved by migration on a 2% agarose gel using 100 bp ladder. **(D):** Correlation between quantity spike-in and *ama-1* expression. *C.elegans ama-1* expression follow a logarithmic function: y=-1.231ln(x)+30.406 with a coefficient of correlation r^2=0.9668. **(E):** Reproducibility of the technique. Following RNA extraction after 75 ng of spike-in total *C.elegans* RNA, *ama-1* expression was determined by qRT-PCR and the results have been displayed as Ct.

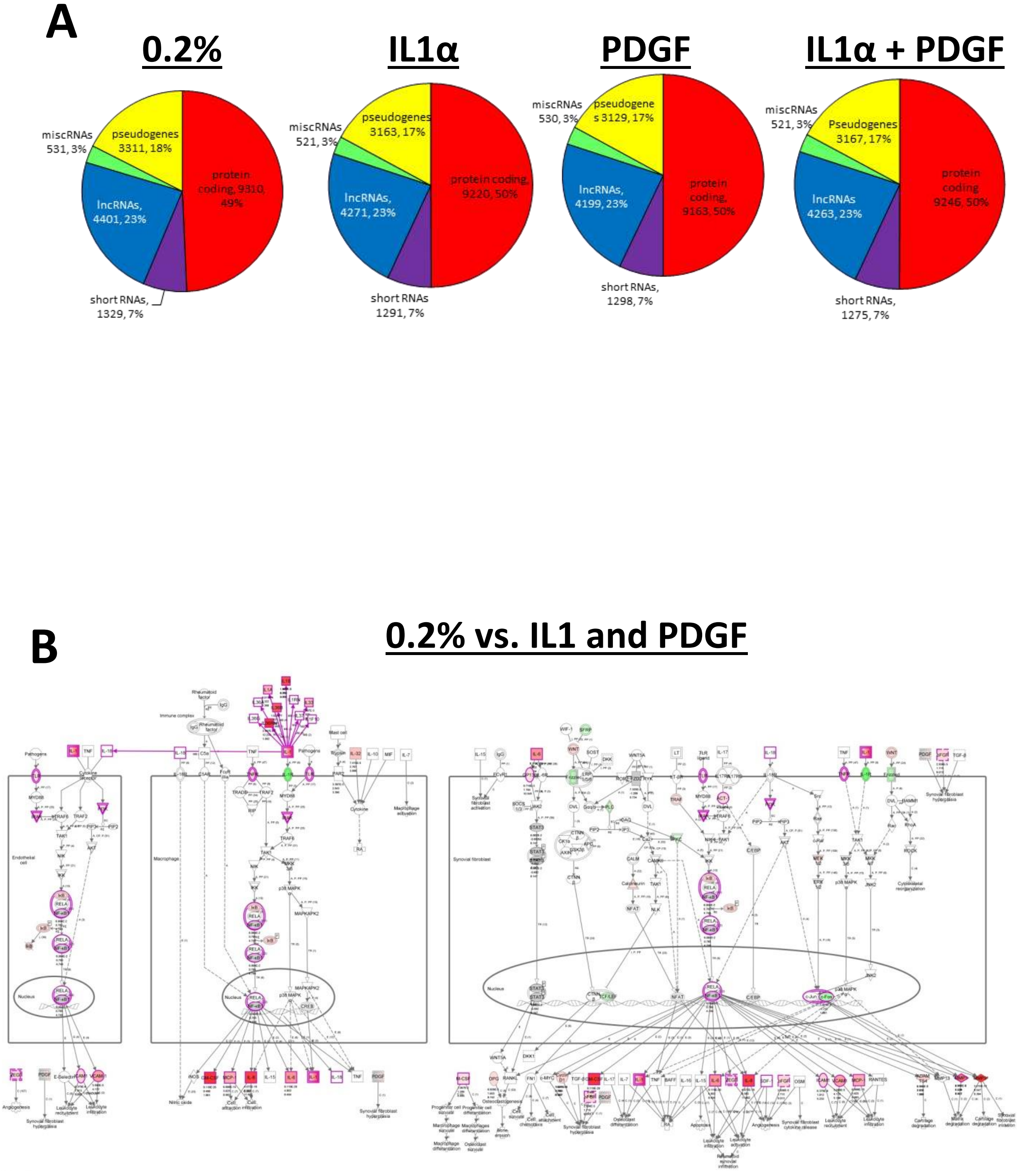

Supplemental Figure 2: **Assessment of RNA-seq data. (A):** Biotype distribution of all transcripts identified by RNA-seq analysis generated from HSVSM cells treated with IL1α and PDGF, cutoff at FPKM>0.1 **(B):** IPA analysis of top protein coding genes following IL1α and PDGF treatment.

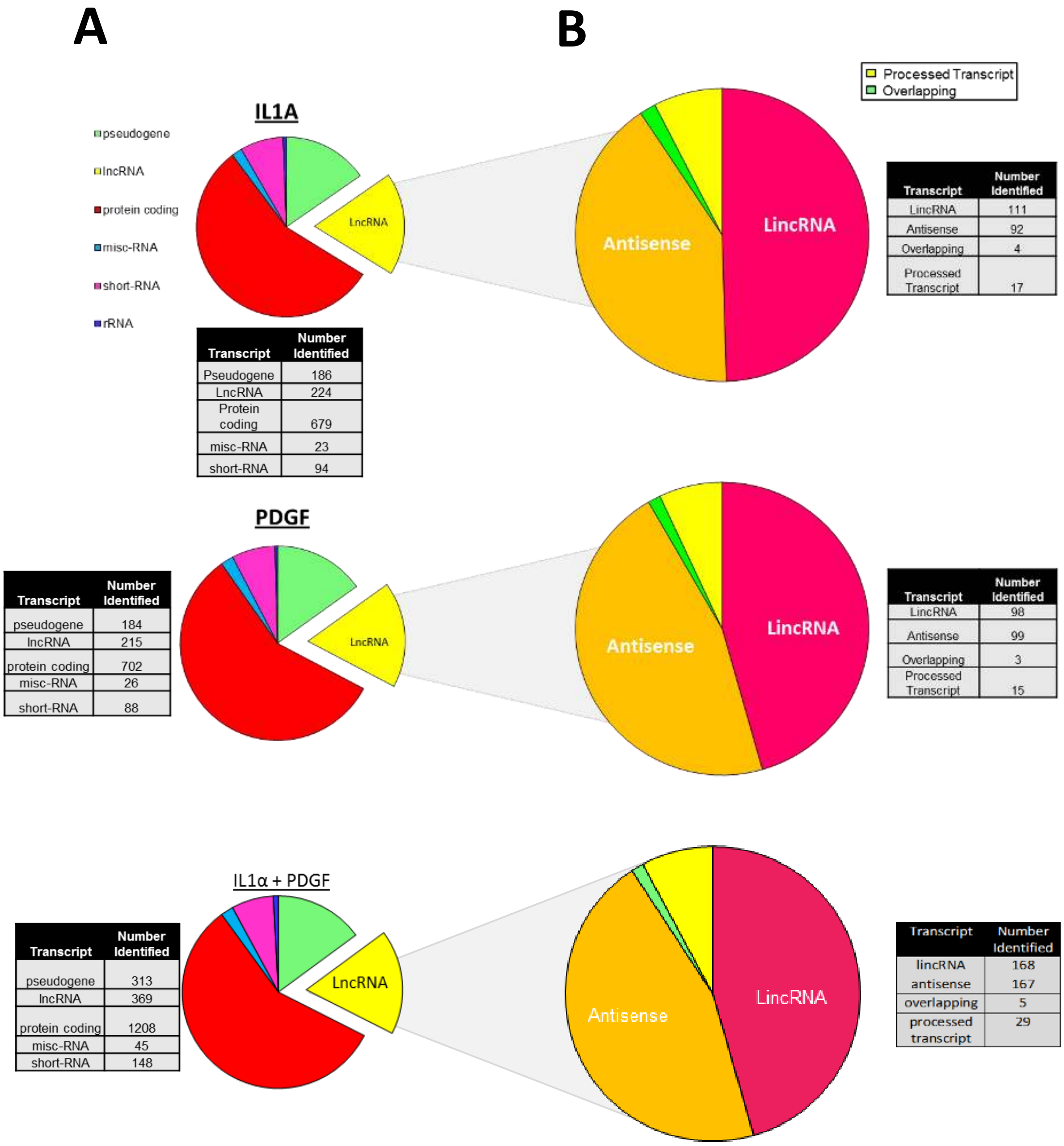

Transcript	Number Identified
Pseudogene	186
LncRNA	224
Protein coding	679
misc-RNA	23
short-RNA	94

Transcript	Number Identified
LincRNA	111
Antisense	92
Overlapping	4
Processed Transcript	17

Transcript	Number Identified
pseudogene	184
lncRNA	215
protein coding	702
misc-RNA	26
short-RNA	88

Transcript	Number Identified
LincRNA	98
Antisense	99
Overlapping	3
Processed Transcript	15

Transcript	Number Identified
pseudogene	313
lncRNA	369
protein coding	1208
misc-RNA	45
short-RNA	148

Transcript	Number Identified
lincRNA	168
antisense	167
overlapping	5
processed transcript	29

Supplemental Figure 3: **Identification of differentially expressed LncRNAs in HSVSMC treated with IL1α and PDGF.** Transcripts differentially expressed between 0.2% and stated treatment ($p<0.01$), pie chart indicates the relative percentage, and tables present numbers, of each biotype differentially expressed. LncRNAs differentially expressed between 0.2% vs IL1α/PDGF can be subdivided based on lncRNA biotype. Groups include intervening lncRNA (lincRNA), antisense, overlapping and processed transcripts.

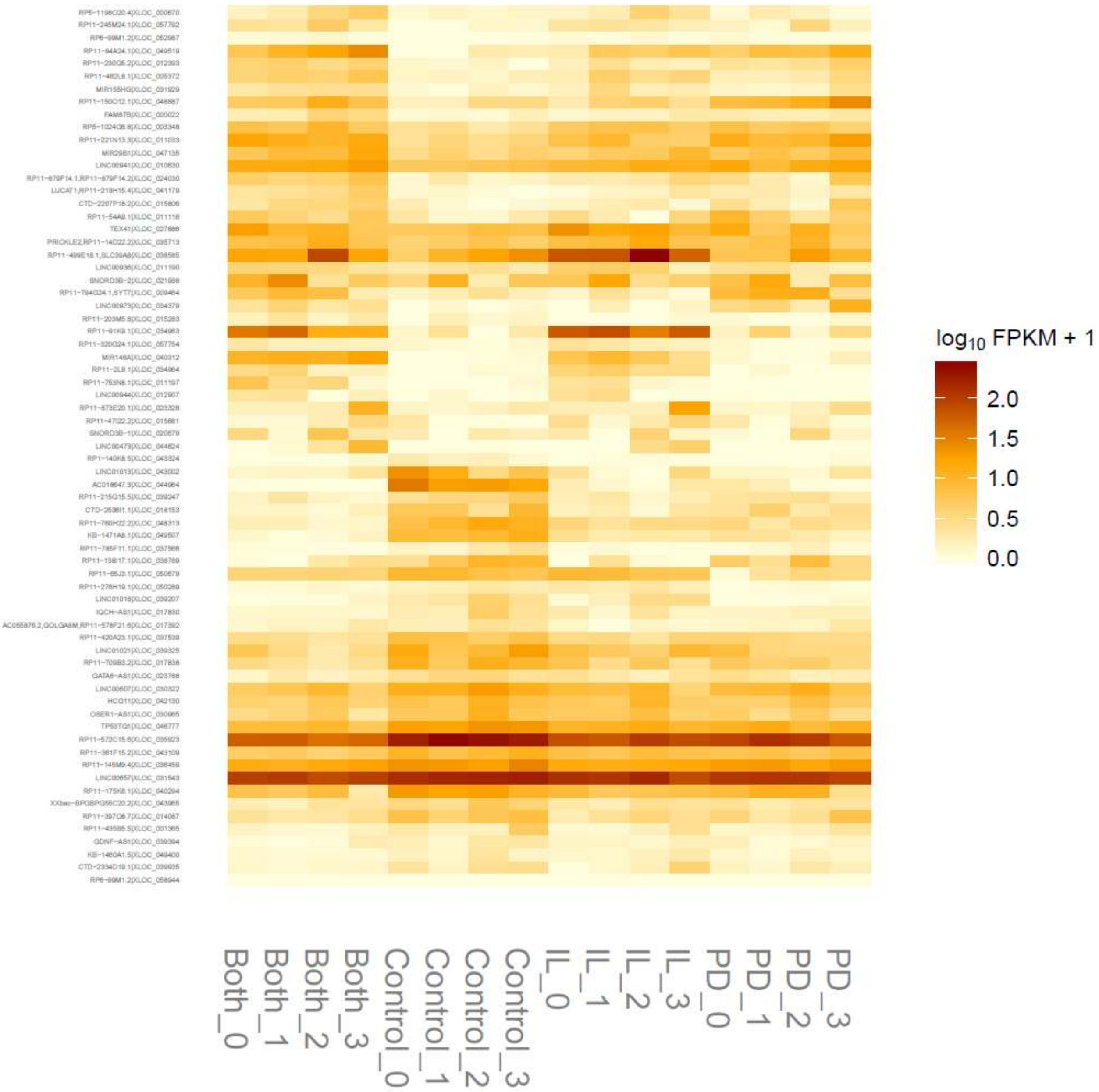

Supplemental Figure 4: **Heat map of most significantly dysregulated intervening lncRNAs across all treatment groups.** Heat map shows most significant changes in intervening lncRNA 0.2% vs IL1+PDGF treatment. LincRNA cut off using FDR<0.01, FPKM>1.

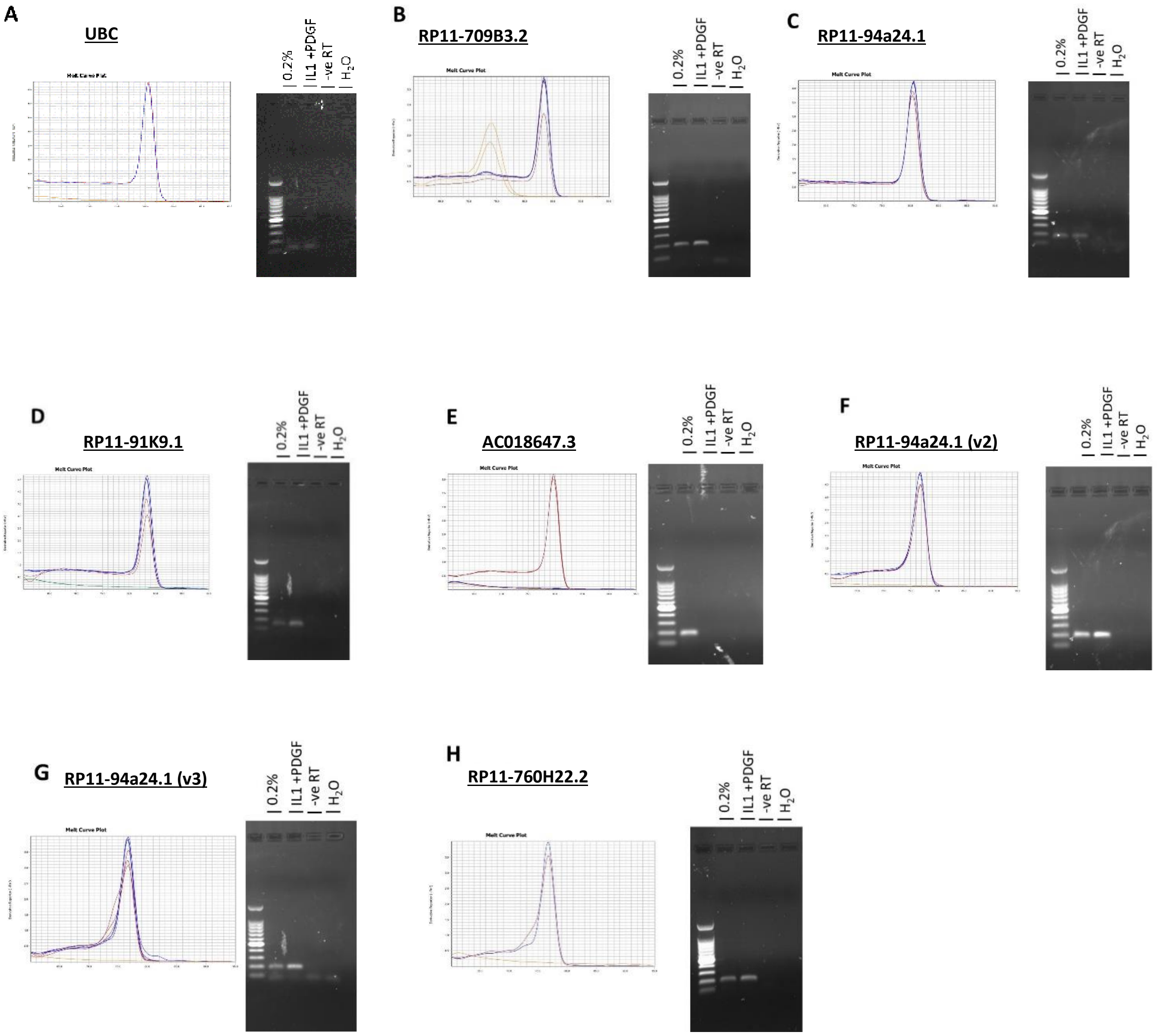

Supplementary Figure 5: Dissociation curves and gel products of PCR reactions indicating single PCR products. (A-H) Dissociation curves and gels for each lncRNA primer set. Primers were tested under 0.2% and IL1+PDGFconditions. Each gel also contains lanes containing –ve RT and H_2O samples.

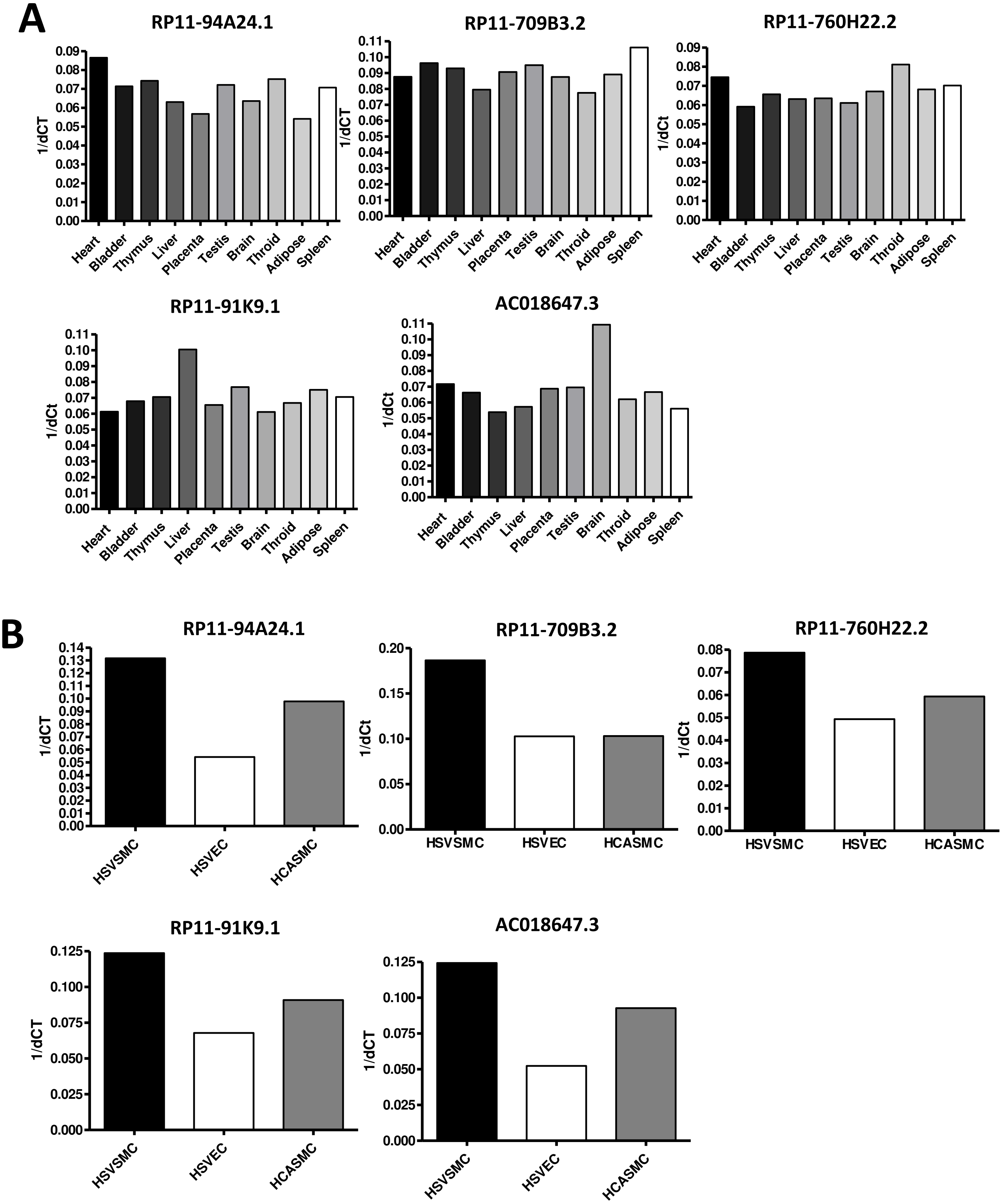

Supplemental Figure 6: LncRNA tissue and cell specificity analysis. (**A**): Expression of LncRNAs in a healthy tissue panel. Expression determined by qRT-PCR and results displayed as 1/ΔCT. (**B**): Expression of lncRNAs in unstimulated HSVSMC, HSVEC or HCAVSMC.

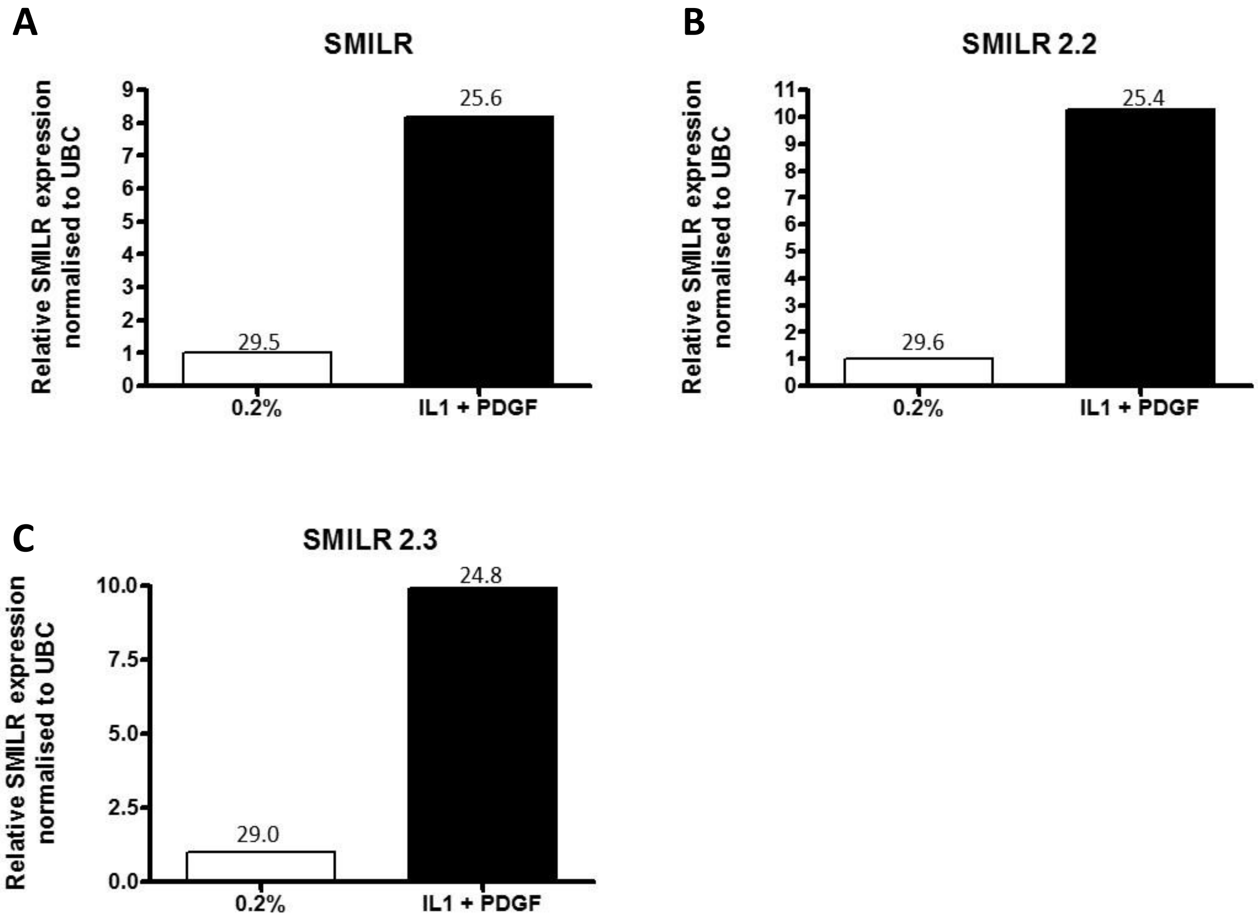

Supplemental Figure 7: Validation of additional SMILR primers. (A-C): Assessment of SMILR via qRT-PCR expression via 3 independent primer sets. The number on top of graphs represent Ct values obtained under 0.2% and dual stimulated conditions.

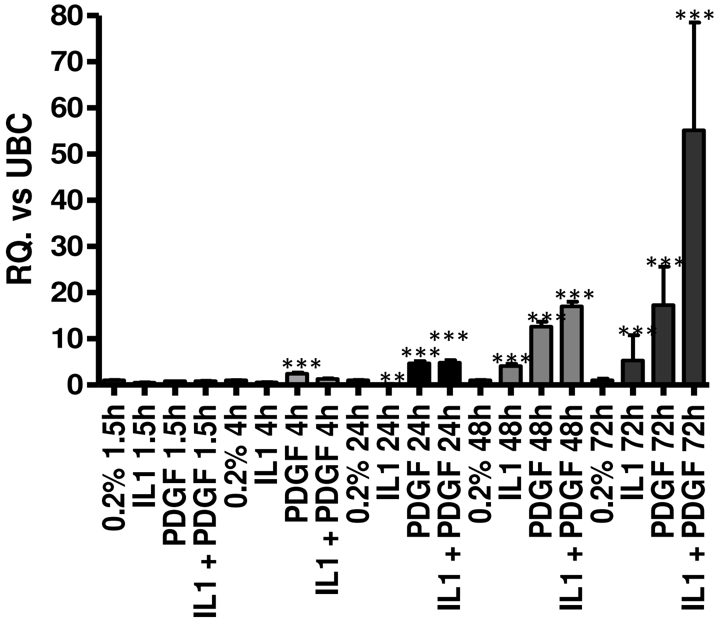

Supplemental Figure 8: **Temporal regulation of lncRNA 2 assessed by qRT-PCR.** HSVSMC were stimulated with IL1α, PDGF of a combination for the stated time points. RNA was extracted and expression determined by qRT-PCR.

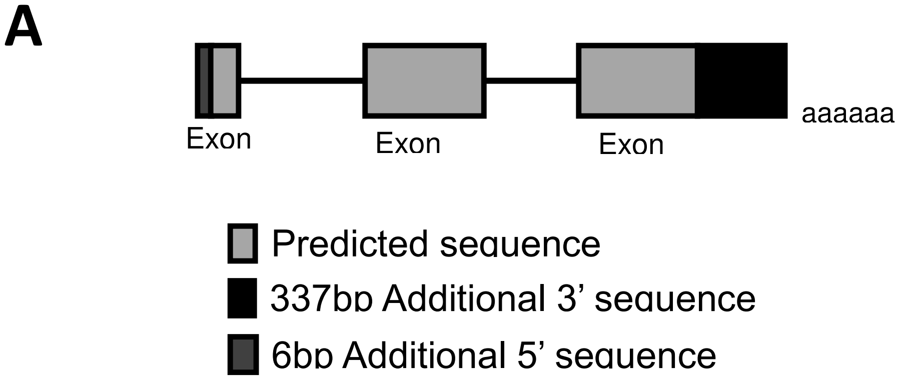

B

RP1194A24.1LncRNA2
GCTGCAAACATTGGGATCAGCCGTGACTATCCCATAACATAATATTTCTGATTTCATTCTTTT
CCTTTCTCCTACCAATTTAATCTGCAATCACTTCAAGAGAAGTCTGTTTAAAGGATATTCACA
TTCTG (intron1-11,398)
TTCACAGAGTTTGAGAGAAACTGTATTCAAGTTGCTGAAACCAAGAAGCTACACTCACGAGT
CTCACCTAAACTCGAATCTGATTTAGATGACATCATCCTGGACTTTGAGTTGATGAAACCTTG
GAGGTCTTGGGAGTAAAGCAAGTGTGATTTGCATATGATGGATATGAATTGTAATGGCCAGA
GCATGGCTGTG (intron 2- 2,269)
AGATGAAAACTCCCATTTTAGGGAACCAAGACTGAATTCCATAATTTACATGGATGTTTGGAA
GGTGTCTGCAACTTAATCTGTGTTCGTTTCTGAGATGTTGGGCAACTCCTTCTTGGAAGATG
TGGTAATGGTCTCTTCGAAAAGAAAATAATCATCTGAGTTTTGGCCAAAATAGTTGATCGGAT
TACCTATGAAAATGACTCTCACCCAACTACAAGAATGTTATGATGTAGAAACTCTAAATATAT
GAGTAATTAACTATACAACACTCCATCCCCATGTGAAAATCTTTAATCTTTTAAGATACTGAAA
TTTTGTGTATGTCTCATAATTTTCTGTATATGGTCAATGAGTTTTGCCTTAGCCATAAGTGGT
CTGTCTGAAATCTTCTCTATTATTTGTGCATTTTCTTCCTGATGTACCAAGCCTAGTCTGTTTG
TTTTTTCCTAAGAGAAAAGCAGATGATTCAACTGTGTATTTCTCAGTGTTGATATTGTGGTTT
GAGGTATTTCATAATCTTGAGTAAAATCTTGTCATAAAAAAAAAAAAAAAAAAAAA

Supplemental Figure 9: **Visual representation of full *SMILR* transcript. (A):**Grey boxes indicate the predicted *SMILR* sequence obtained from UCSC genome browser (RP11-94A24.1) . Black boxes represent additional 316 basepair sequence obtained via 3' RACE of *SMILR* transcript. ***P<0.001, ** P<0.01 and * P<0.05 vs 0.2% in each time point (1 way ANOVA). **(B):** Full length sequence of lncRNA 2.

A

SMILR Raw RNA-seq Reads – Control (0.2%) and stimulated (IL1 + PDGF)

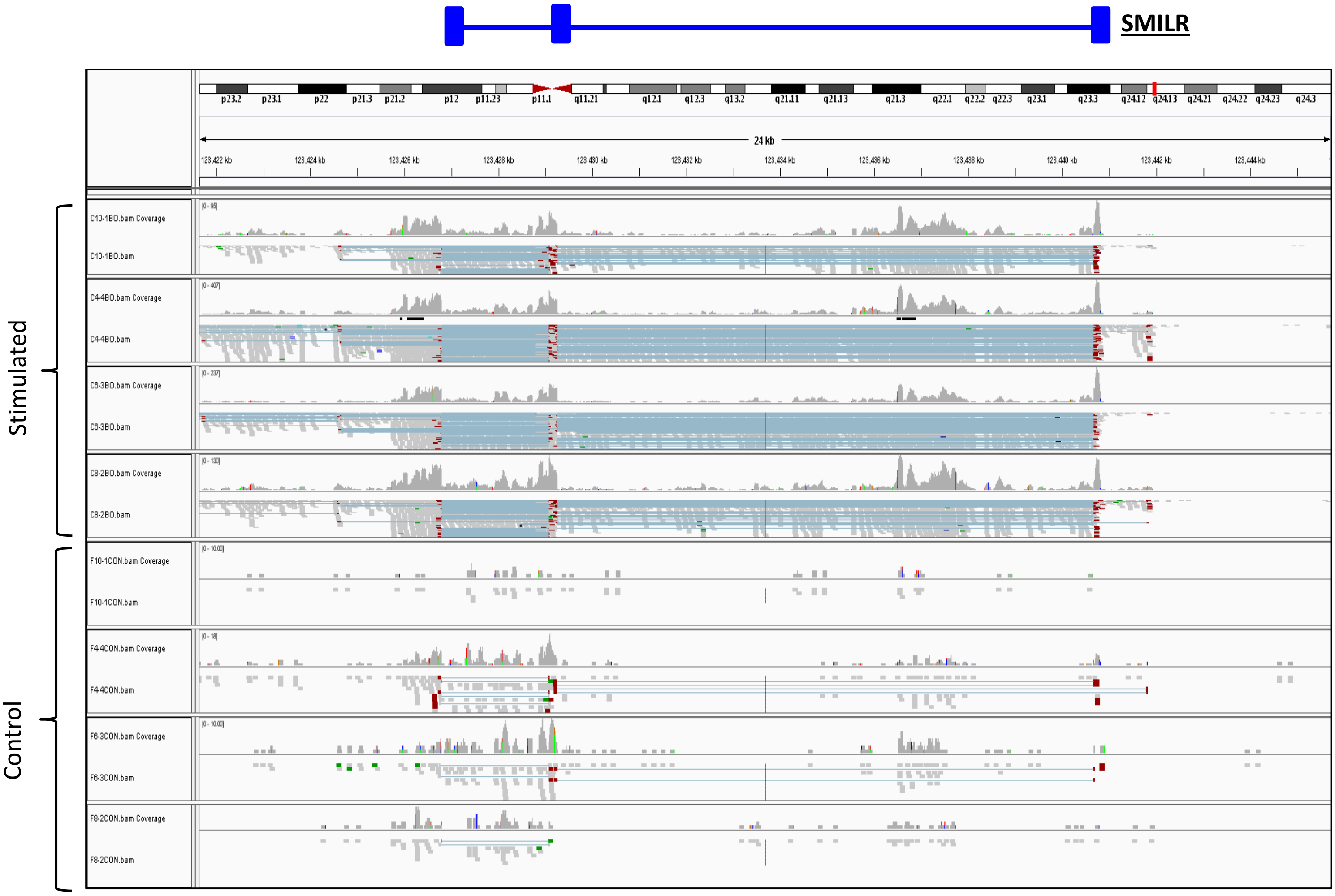

B *HAS2 Raw RNA-seq Reads – Control (0.2%) and stimulated (IL1 + PDGF)*

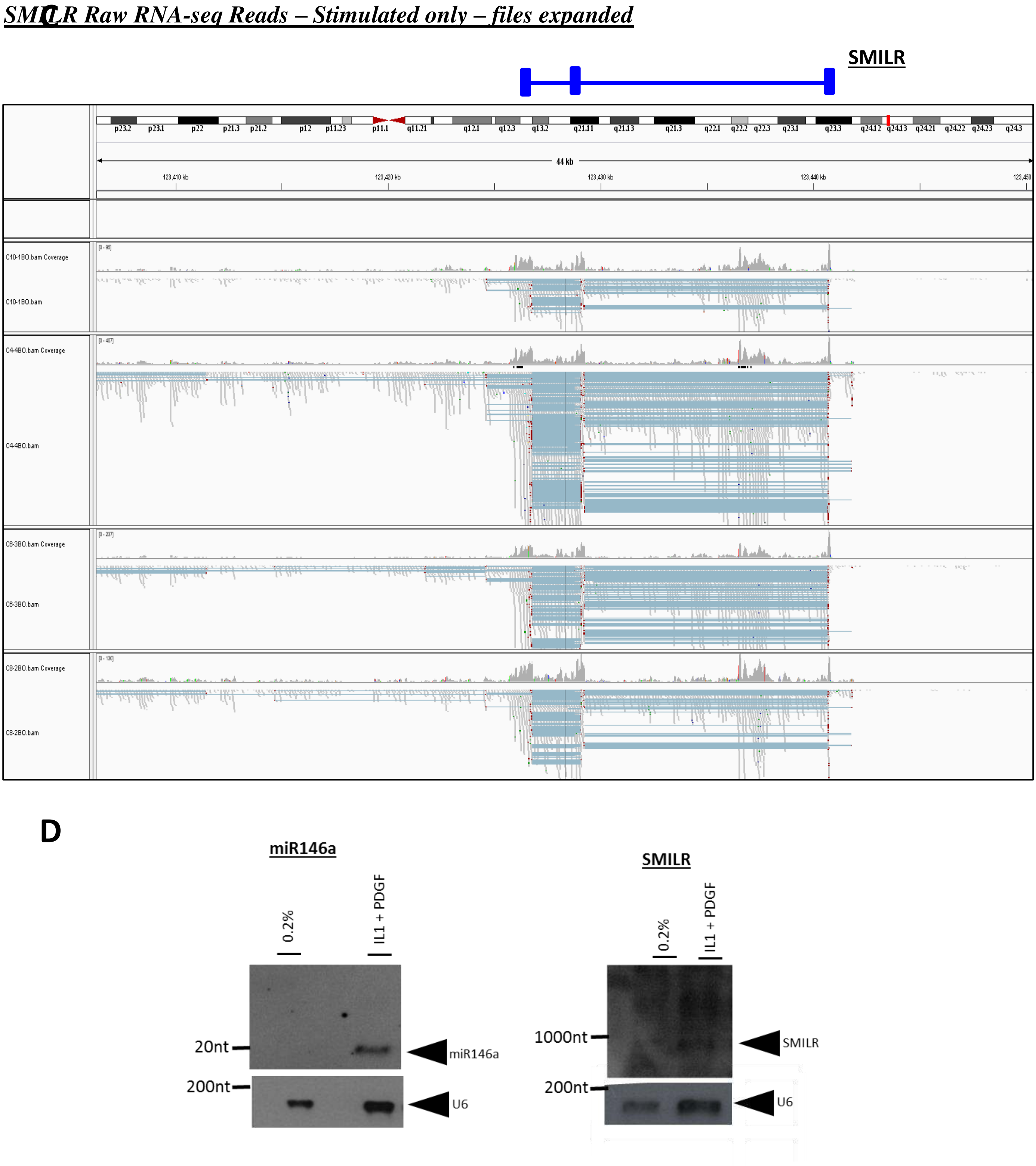

Supplemental Figure 10: Raw sequencing profiles generated utilising tophat files, constructed on integrative genome viewer (IGV). (A): Raw sequencing reads of SMILR under both basal and dual stimulated (IL1 + PDGF) conditions n=4. **(B):** Raw sequencing reads of HAS2 indicating a similar expression pattern following stimulation. **(C):** Raw sequencing reads of SMILR under stimulated conditions – expanded **(D):** Northern analysis of miR146a and SMILR RNA. U6 shown as loading control.

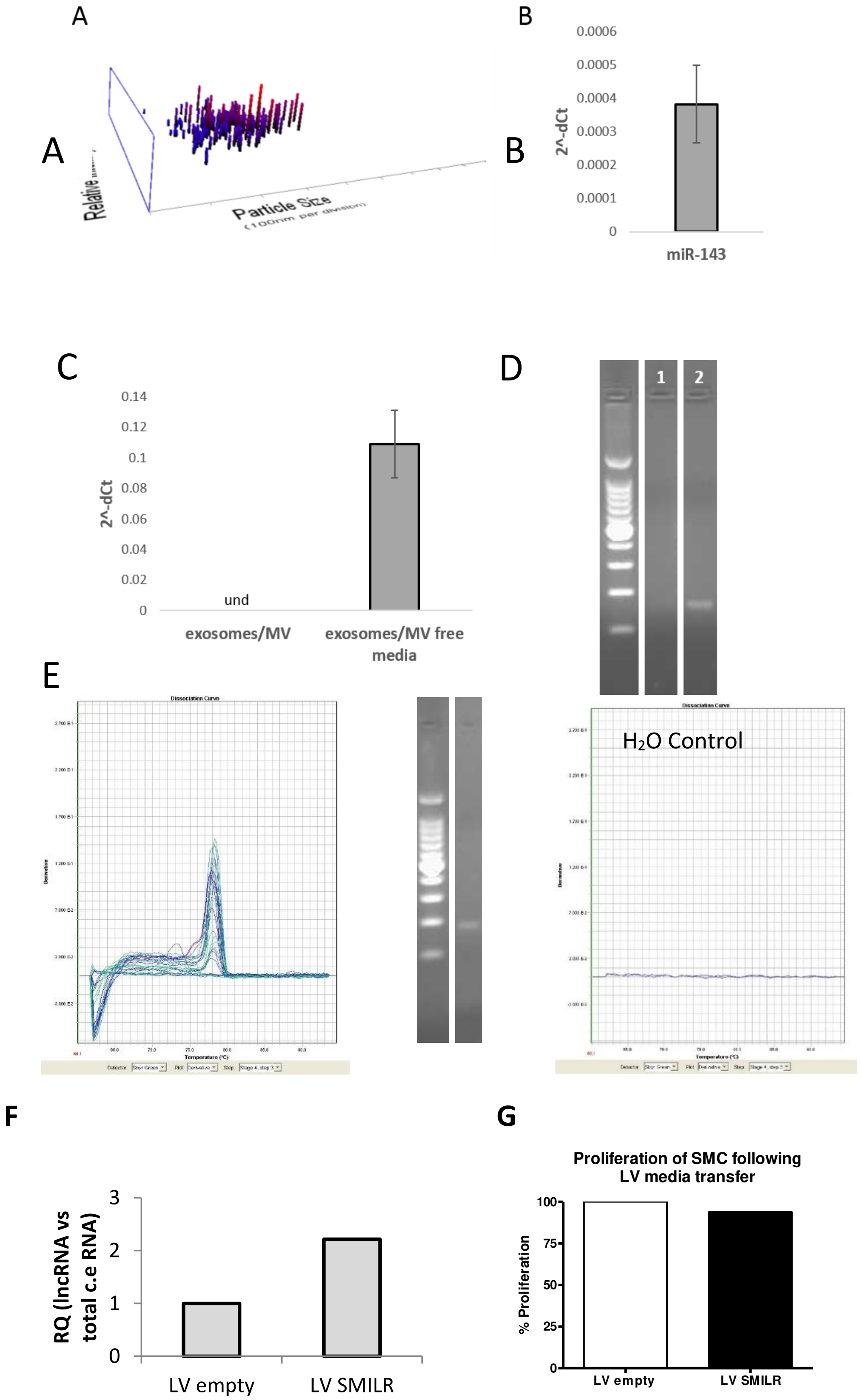

Supplemental Figure 11: Exosome isolation from HSVSMC conditioned media. (A): Size evaluation using the Nanosight of exosomes and MV isolated using the Total exosome isolation kit from 0.2% conditioned media. Sizes obtained between 70 and 600 nm. **(B):** Quantification of miR-143 in exosomes/MV isolated using the Total exosome isolation kit from 0.2% conditioned media. **(C):** SMILR expression analysed by qRT-PCR in exosomes/MV and exosomes/MV free media compartment from IL-1α + PDGF conditioned media. **(D):** Agarose gel of qRT-PCR products obtained in C; 1: exosomes/MV compartment, 2: exosomes/MV free media. **(E):** melting curves and gel electrophoresis of SMILR primer set in conditioned media**. (F):** SMILR expression from conditioned media following control lentivirus or SMILR lentivirus infection of cells. **(G):** Subsequent proliferation of quiesced cells following 48h incubation with lentivirus conditioned media.

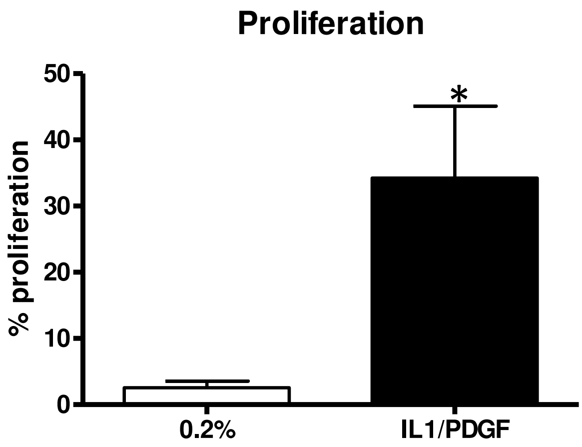

Supplemental Figure 12: Proliferation of HSVSMC 0.2% vs IL1 + PDGF treatment. P<0.05 students t test.

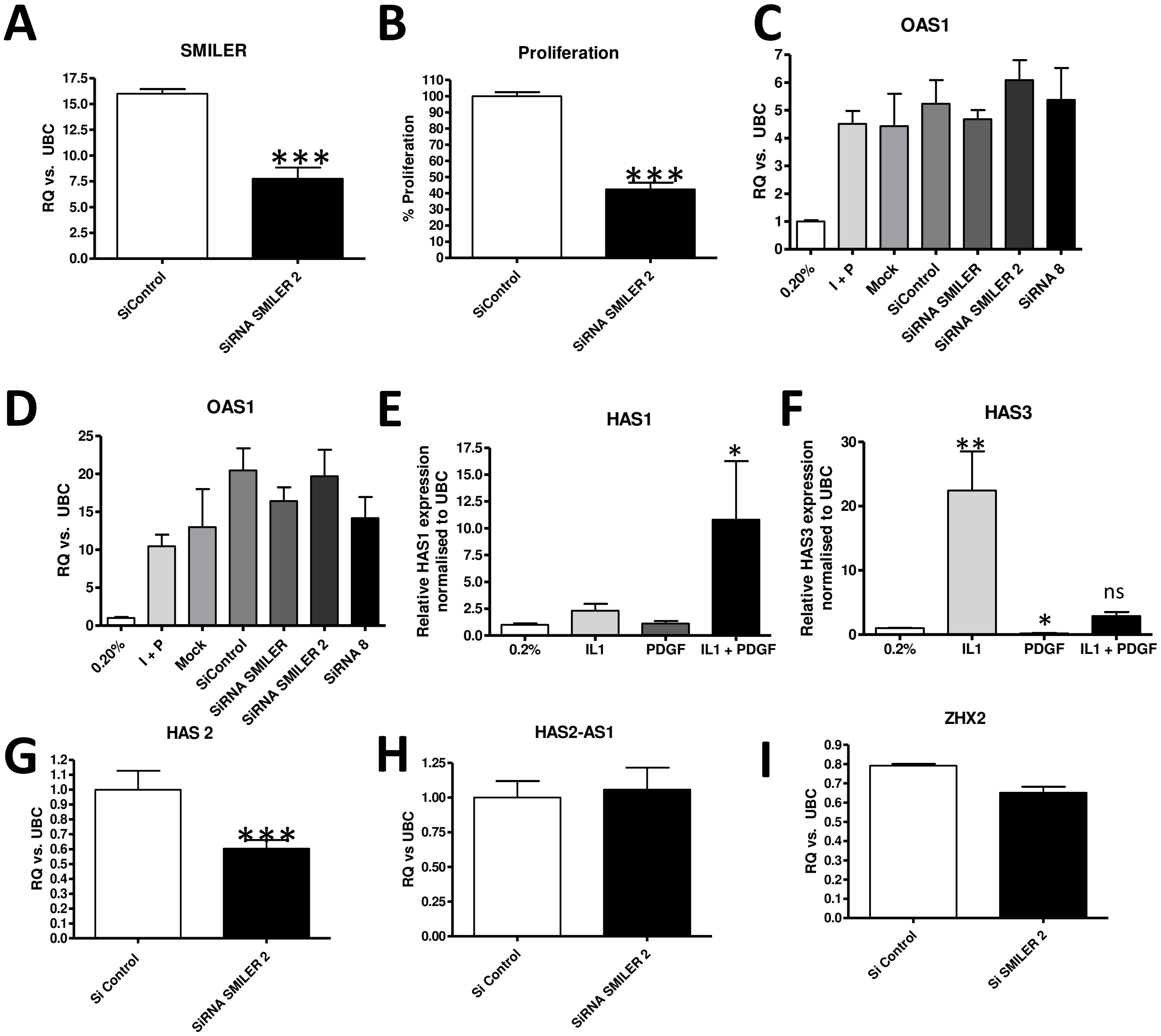

Supplemental Figure 13: (A): Confirmation of siRNA mediated down regulation of *SMILR* using second siRNA targeting a separate sequence of *SMILR*. **(B):** Confirmation of knockdown of *SMILR* using second siRNA. Analysed by students t-test ****P*<0.001 vs SiControl. **(C-D):**qRT-PCR analysis of interferon gamma associated mRNA *OAS1* and *IRF7*. **(E-F):** qRT-PCR validation of *HAS1* and *HAS3* regulation by IL1α and PDGF. One way ANOVA *P<0.05. **(G-I):** Validation of siSMILR using second siRNA targeting different section of the lncRNA.

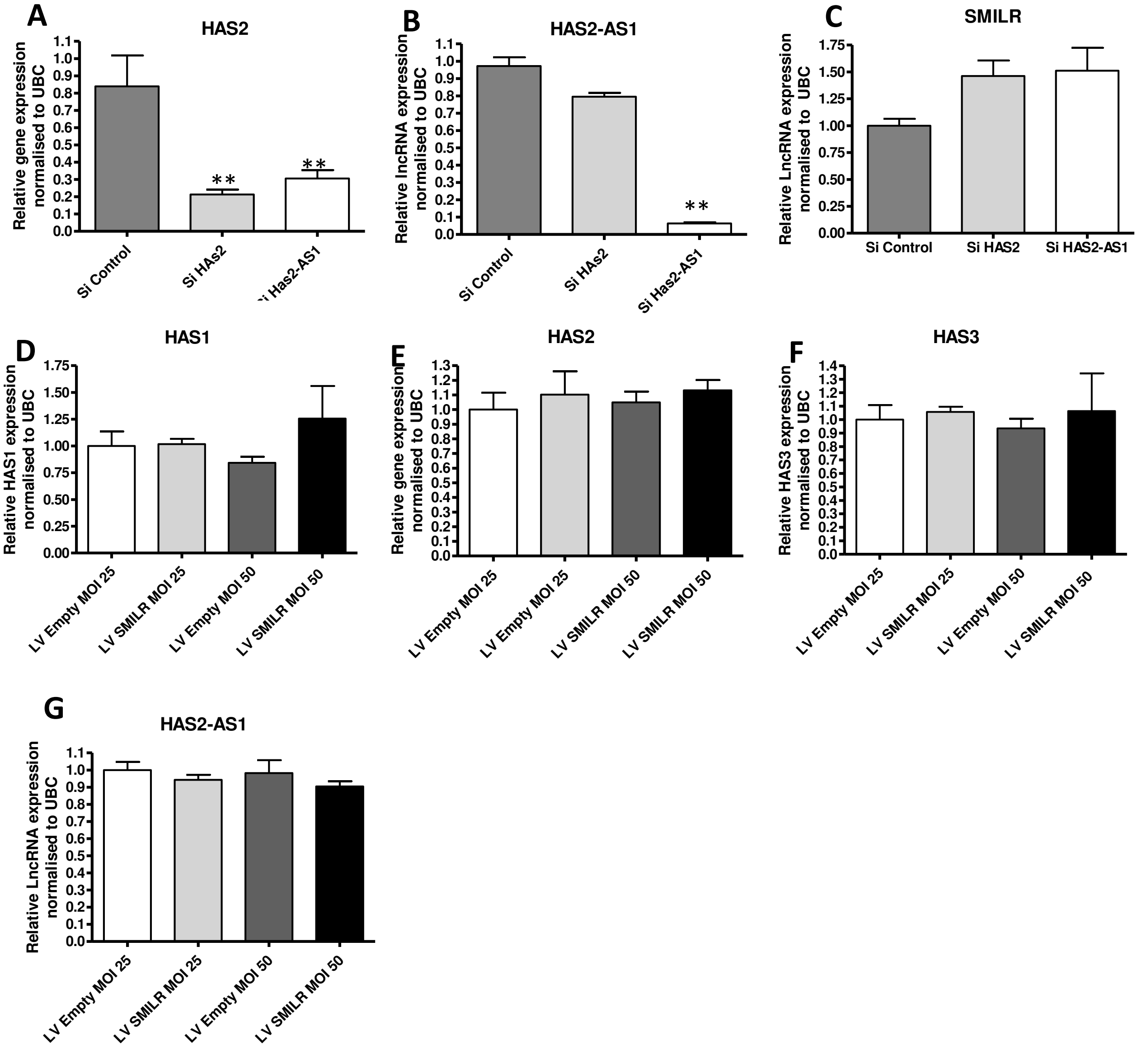

Supplemental Figure 14: Effect of HAS2 and HAS2-AS1 knockdown on SMILR expression. (A): Knocdown of HAS2 or HAS2-AS1 both reduced HAS2 expression. **(B):** Knockdown of neither HAS2 nor HAS2-AS1 affected SMILR expression levels. **(C):** Knockdown of HAS2 –AS but not HAS2 significantly reduced HAS2-AS1levels. **(D-F):** Overexpression of SMILR did not affect HAS1-HAS3 nor HAS1-AS1 expression levels.

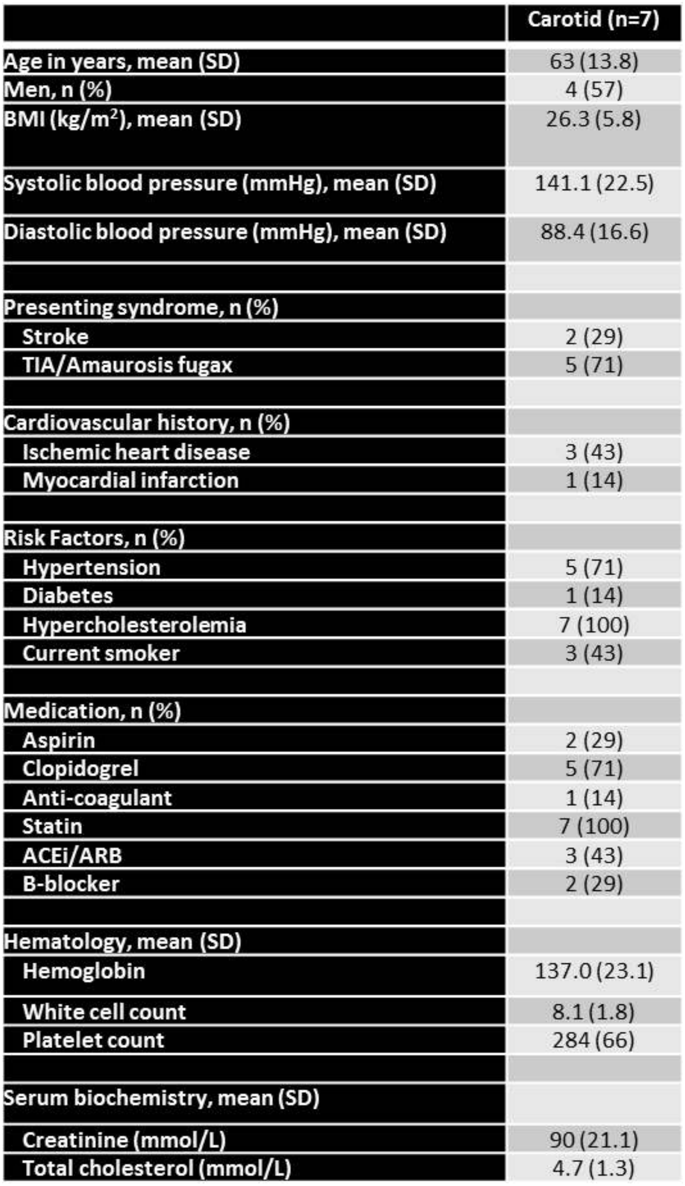

	Carotid (n=7)
Age in years, mean (SD)	63 (13.8)
Men, n (%)	4 (57)
BMI (kg/m^2), mean (SD)	26.3 (5.8)
Systolic blood pressure (mmHg), mean (SD)	141.1 (22.5)
Diastolic blood pressure (mmHg), mean (SD)	88.4 (16.6)
Presenting syndrome, n (%)	
Stroke	2 (29)
TIA/Amaurosis fugax	5 (71)
Cardiovascular history, n (%)	
Ischemic heart disease	3 (43)
Myocardial infarction	1 (14)
Risk Factors, n (%)	
Hypertension	5 (71)
Diabetes	1 (14)
Hypercholesterolemia	7 (100)
Current smoker	3 (43)
Medication, n (%)	
Aspirin	2 (29)
Clopidogrel	5 (71)
Anti-coagulant	1 (14)
Statin	7 (100)
ACEi/ARB	3 (43)
B-blocker	2 (29)
Hematology, mean (SD)	
Hemoglobin	137.0 (23.1)
White cell count	8.1 (1.8)
Platelet count	284 (66)
Serum biochemistry, mean (SD)	
Creatinine (mmol/L)	90 (21.1)
Total cholesterol (mmol/L)	4.7 (1.3)

Supplemental Table 5- Baseline Patient Characteristics – Carotid Cohorts.

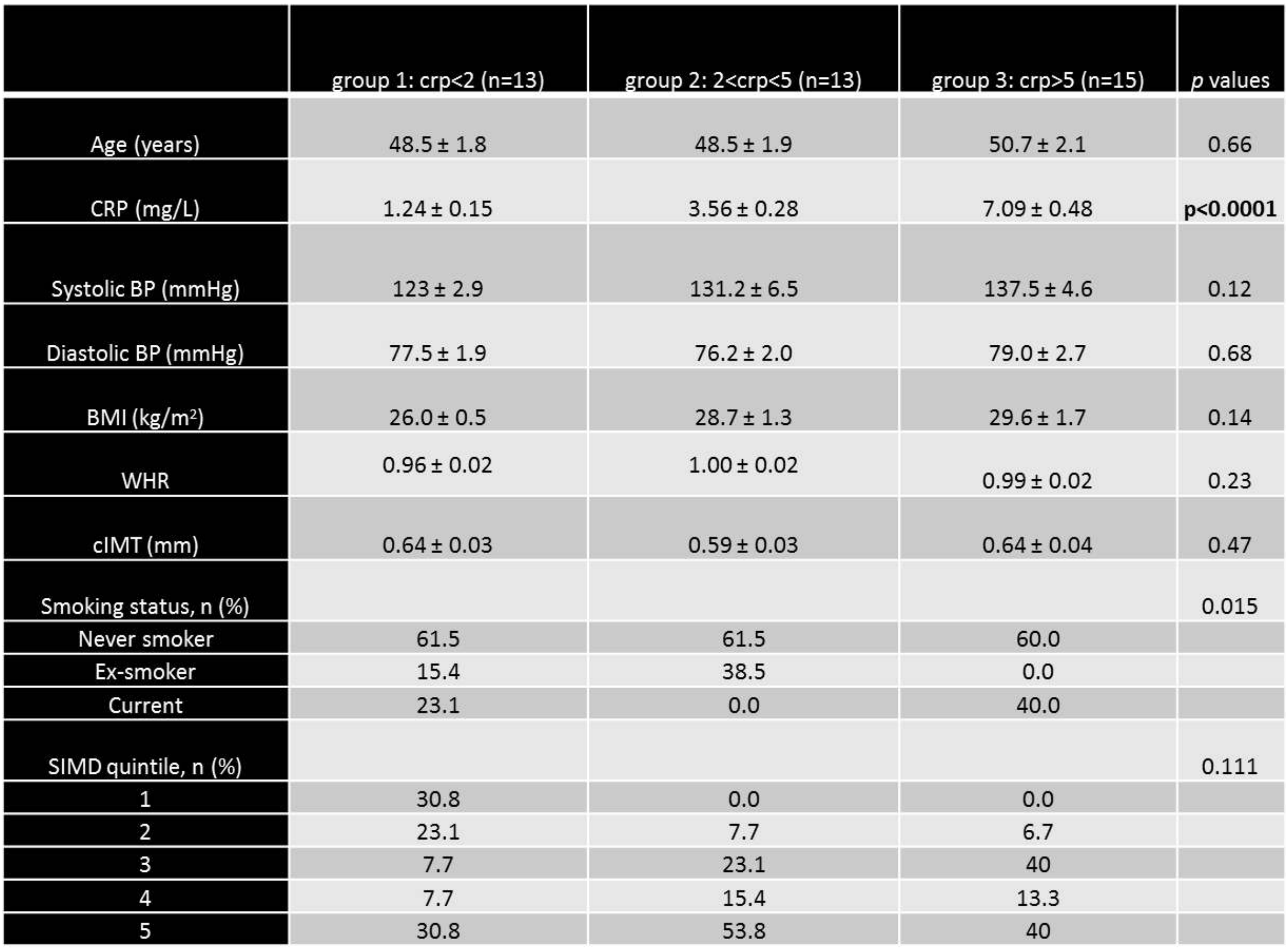

	group 1: crp<2 (n=13)	group 2: 2<crp<5 (n=13)	group 3: crp>5 (n=15)	*p* values
Age (years)	48.5 ± 1.8	48.5 ± 1.9	50.7 ± 2.1	0.66
CRP (mg/L)	1.24 ± 0.15	3.56 ± 0.28	7.09 ± 0.48	**p<0.0001**
Systolic BP (mmHg)	123 ± 2.9	131.2 ± 6.5	137.5 ± 4.6	0.12
Diastolic BP (mmHg)	77.5 ± 1.9	76.2 ± 2.0	79.0 ± 2.7	0.68
BMI (kg/m^2)	26.0 ± 0.5	28.7 ± 1.3	29.6 ± 1.7	0.14
WHR	0.96 ± 0.02	1.00 ± 0.02	0.99 ± 0.02	0.23
cIMT (mm)	0.64 ± 0.03	0.59 ± 0.03	0.64 ± 0.04	0.47
Smoking status, n (%)				0.015
Never smoker	61.5	61.5	60.0	
Ex-smoker	15.4	38.5	0.0	
Current	23.1	0.0	40.0	
SIMD quintile, n (%)				0.111
1	30.8	0.0	0.0	
2	23.1	7.7	6.7	
3	7.7	23.1	40	
4	7.7	15.4	13.3	
5	30.8	53.8	40	

Supplemental Table 6- Baseline Patient Characteristics – CRP matched plasma samples. Values are represented in mean ± SEM with *p* values calculated by one-way ANOVA or by Fisher's exact test for categorical variables.

SMILR in plasma

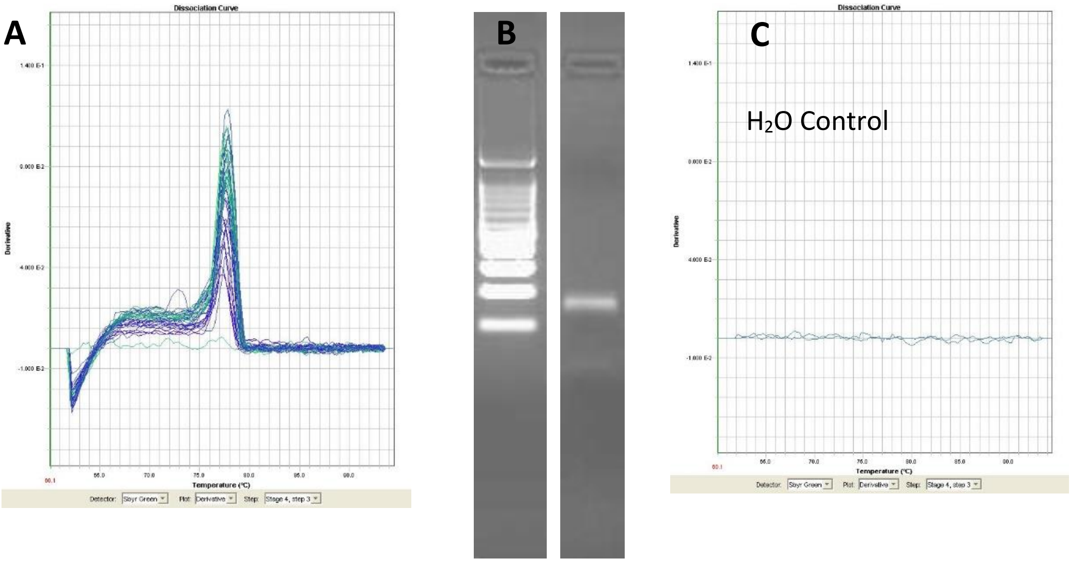

Detector: Sbyr Green Plot: Derivative Step: Stage 4, step 3

Supplemental Figure 15: Primer validation and quality control in plasma samples. **(A):** Melting curve for SMILR in plasma. **(B):** Agarose gel of qPCR product. **(C):** Water melting curve.

A The Pearson correlation:

		crp trans dct
Crp	1.0000	
Transdct	0.5719 0.0001	1.0000

So r=0.5719, r2=0.327, p<0.001

B If we take out the two outliers (the two highest dCts):

```
pwcorr crp transdct, sig
```

		crp trans dct
Crp	1.0000	
Transdct	0.389 0.0144	1.0000

r=0.389, r^2=0.151, p=0.014

Supplemental Figure 16: Statistical analysis of SMILR vs. CRP correlation. (A): Pearson correlation of SMILR vs. CRP utilising all data points. R=0.5719, r^2=0.327 and P<0.001. **(B):** Pearson correlation of SMILR vs. CRP omitting the 2 highest outlying points. R=0.389, r^2=0.151, p=0.014.

Supplemental References

1. Billings FTt, Balaguer JM, C Y, Wright P, Petracek MR, Byrne JG, Brown NJ, Pretorius M. Comparative effects of angiotensin receptor blockade and ace inhibition on the fibrinolytic and inflammatory responses to cardiopulmonary bypass. *Clinical pharmacology and therapeutics*. 2012;91:1065-1073
2. Hathout GM, Fink JR, El-Saden SM, Grant EG. Sonographic nascet index: A new doppler parameter for assessment of internal carotid artery stenosis. *AJNR. American journal of neuroradiology*. 2005;26:68-75
3. Upadhyay S, Ganguly K, Stoeger T, Semmler-Bhenke M, Takenaka S, Kreyling WG, Pitz M, Reitmeir P, Peters A, Eickelberg O, Wichmann HE, Schulz H. Cardiovascular and inflammatory effects of intratracheally instilled ambient dust from augsburg, germany, in spontaneously hypertensive rats (shrs). *Particle and fibre toxicology*. 2010;7:27
4. Irkle A, Vesey AT, Lewis DY, Skepper JN, Bird JL, Dweck MR, Joshi FR, Gallagher FA, Warburton EA, Bennett MR, Brindle KM, Newby DE, Rudd JH, Davenport AP. Identifying active vascular microcalcification by (18)f-sodium fluoride positron emission tomography. *Nature communications*. 2015;6:7495
5. Armand-Labit V, Meyer N, Casanova A, Bonnabau H, Platzer V, Tournier E, Sansas B, Verdun S, Thouvenot B, Hilselberger B, Doncescu A, Lamant L, Lacroix-Triki M, Favre G, Pradines A. Identification of a circulating microrna profile as a biomarker of metastatic cutaneous melanoma. *Acta dermato-venereologica*. 2016;96:29-34